heritage

MDPI

Article

Degradation of Traditional Silicate Glass and Protective Coatings Under Simulated Unsheltered Conditions

Sofia Schiattone [1,†], Elisabetta Tomiato [1], Elena Bernardi [2,3,*], Martina Zangari [2], Tommaso Salzillo [2], Mariangela Vandini [1] and Cristina Chiavari [1,*]

[1] Department of Cultural Heritage, Alma Mater Studiorum—University of Bologna, Via Degli Ariani 1, 40121 Ravenna, Italy; sofiaschiattone96@gmail.com (S.S.); elisabetta.tomiato2@unibo.it (E.T.); mariangela.vandini@unibo.it (M.V.)
[2] Department of Industrial Chemistry Toso Montanari, Alma Mater Studiorum—University of Bologna, Via Piero Gobetti 85, 40129 Bologna, Italy; martina.zangari@unibo.it (M.Z.); tommaso.salzillo@unibo.it (T.S.)
[3] Center for Industrial Research-Fonti Rinnovabili, Ambiente, Mare e Energia (CIRI FRAME), Alma Mater Studiorum—University of Bologna, Via D. Campana 71, 47923 Rimini, Italy
* Correspondence: elena.bernardi@unibo.it (E.B.); cristina.chiavari@unibo.it (C.C.)
† Present address: Coopera Heritage Conservation, Via Germanico 107, 00192 Roma, Italy.

Abstract

Outdoor glass is subject to degradation due to environmental factors, which alter its physical and chemical properties depending on the exposure conditions. Studying glass weathering and the effectiveness and durability of conservation treatments is necessary for developing optimal conservation strategies for glass heritage objects. Here, an accelerated aging protocol based on actual environmental data is successfully employed to replicate weathering caused by rain runoff, temperature, humidity and UVA radiation in unsheltered conditions. Two types of silicate glass with traditional compositions were artificially aged to investigate the corrosion processes and produce representative weathered substrates for applying and aging protective treatments. The performance of two recently marketed Siox-5 sol–gel systems was compared with that of Paraloid B72. Glass specimens, as well as leaching rain solutions, were analyzed with different techniques, including SEM/EDS, FTIR-ATR, color measurements and MP-AES. The composition of the glass influences weathering patterns, which in turn affect coating adhesion and overall performance. Sol–gel coatings demonstrate good chemical stability and tend to adhere more effectively to degraded surfaces than to well-preserved ones. The coatings exhibit varying degrees of sensitivity to environmental factors, with one of the sol–gel systems generally performing better than the others under the considered exposure conditions.

Keywords: ancient glass; colored glass; artificial aging; rain runoff; consolidants; corrosion; cultural heritage; conservation

Academic Editor: Márcia Vilarigues

Received: 30 September 2025
Revised: 5 December 2025
Accepted: 15 December 2025
Published: 20 December 2025

1. Introduction

Through history, countless artistic objects and items for everyday use have been made of silicate glass. Glass is an amorphous material made through the fusion and rapid cooling of mineral mixtures. Glass may be defined as a supercooled melt, which is in metastable thermodynamic equilibrium at the temperature of use. The structure of silicate glass can be described as a random network of SiO_4 tetrahedrons. Along the main network, other oxides are added, and elements of these oxides break up some of the Si–O–Si bonds, creating non-bridging oxygens (NBOs). In glass chemistry, Q_n notation is used to describe the

number of bridging oxygens (BOs) bonded to a Si atom, where n ranges from 0 to 4. For example, Q_3 represents a Si site where three O atoms act as BOs and one as NBO [1,2].

Traditional ancient glass was not pure silicate, since different modifiers were added, either intentionally or not. The addition of alkali oxides like Na_2O and K_2O introduces highly mobile monovalent ions that largely decrease viscosity and are thus called fluxing agents [1–3]. Meanwhile, the addition of oxides of alkaline earths introduces divalent ions into the melt, each of which breaks up two Si-O bonds and connects to two NBOs. Therefore, the breakdown of the Si–O–Si bonds is compensated by the introduction of divalent ions [4]. For this reason, such elements tend to have a stabilizing effect on the glass, improving durability and chemical resistance [2,3,5]. PbO was also frequently added to glass. It acts as a fluxing agent, lowering the viscosity of the glass melt, improves chemical resistance and increases the refractive index of the final glass [5–7]. The role of Pb^{2+} in the glass network differs from that of other divalent ions because of its peculiar electronic configuration, which assimilates it to a network former [1,5,7]. Other oxides were frequently added to alter the esthetic properties of the glass, conferring different opacity and colors [2,5].

Glass is susceptible to atmospheric weathering, the main environmental factor affecting its durability being the presence of water. Therefore glass is susceptible to the action of rain, as well as temperature and relative humidity cycles that cause the condensation of moisture on glass [8–13]. The pH of the aqueous solution defines two different degradation mechanisms.

The first corrosion phenomenon is the leaching of modifier ions, particularly that of alkali ions, which, as mentioned, are more mobile. When glass is in contact with an aqueous solution with pH < 9, ions leach out of the glass network, while at the same time, to maintain electrical balance, H^+ ions diffuse into the glass, forming silanol groups. This causes the formation of a layer of altered glass impoverished in modifier ions; this process is also called de-alkalinization [2,3,8,14,15]. Leaching severity depends not only on the composition of the aqueous solution, but also on the composition of the glass itself. The concentration of silica in a glass composition influences the connectivity of non-bridging oxygens (NBOs), affecting the mobility and exchange of ions within the glass network. Glasses with lower silica concentrations have interconnected NBOs, allowing ion movement, while glasses with higher silica concentrations have isolated NBOs, restricting ion mobility. This has implications for the chemical and physical properties of the glass, such as its reactivity and ionic conductivity [3,16]. Moreover, ionic bonds between negatively charged NBOs and modifier ions become weaker as the field intensity of the modifier ion decreases. Field intensity is determined by the charge/size ratio. This determines some preferentiality in the leaching of different elements. Monovalent alkali ions (which bind one NBO) are generally more easily leached out than bivalent ions (which are bonded to two NBOs), and high-radius ions are more easily leached than smaller ions having the same charge. This explains the lower durability of potash-based glass compared to soda silicate glass, with K^+ ions having larger radii than Na^+, and, therefore, being more easily leached out from glass [4].

As the thickness of the altered layer grows, the rate of leaching tends to slow down, as ions need to diffuse through it [2,3,8]. Protons are smaller than the modifier ions previously present in the network, and they form stronger covalent bonds to oxygen atoms; therefore, this exchange results in a contraction and weakening of this glass layer [2]. This is especially true for the high-radius K^+ cations, whose exchange leaves large voids, facilitating water penetration [3].

Moreover, the ion exchange reaction causes an increase in the pH of the aqueous solution, which could lead to the second type of corrosion mechanism.

When pH of water in contact with glass is >9, dissolution of the silica network is favored. As the SiO_4 sites in silicate glasses are susceptible to nucleophilic attack, the OH^- ions present in an alkaline solution can attack the Si-O-Si bonds, dissolving the glass [2,15,17,18]. This reaction causes the formation of a new NBO, which can interact with water, forming further silanol bonds and hydroxyl ions and favoring further silica dissolution [18]. Glass with more NBOs, such as lower silica glass, is more susceptible to this type of weathering, as site reactivity follows the trend $Q_1 > Q_2 > Q_3 > Q_4$ [17].

Therefore, exposure to environmental factors can trigger various deterioration effects on glass surfaces, including surface dulling, iridescent sheens, opalescence, crizzling, pitting, cracking, discoloration and even a complete loss of the material's vitreous character. In the recent years, to mitigate the weathering of historical glass artifacts, conservators and restoration professionals have tended to adopt a preventive conservation approach, aiming to limit direct intervention on original objects [19].

The most common approach adopted in glass conservation is the use of protective coatings and consolidating products, which may be of either organic or inorganic nature [20]. Prior to the advent of synthetic polymers, natural organic substances such as animal glue [21] and shellac [22] were commonly used to consolidate and coat archeological and historical glass. From the mid-20th century onward, advances in polymer chemistry introduced a range of more suitable synthetic materials for conservation purposes. These included early cellulose derivatives, soluble nylon, vinyl resins, epoxy resins and acrylic resins (among them, the widely adopted Paraloid B72) [19]. Despite their initial promise, these materials have revealed several limitations over time, particularly in their ability to withstand environmental stressors such as temperature and humidity fluctuations, as well as exposure to solar radiation. Moreover, the majority are solvent-based, posing health risks to conservators and environmental concerns [19,23].

Currently, the most widely used and advanced glass coatings are silica-based, produced through the synthetic sol–gel process. Sol–gel is a flexible technique for creating solid materials from tiny molecules and can be used to create thin films or coatings on glass or ceramic materials. A sol, which is a colloidal solution of particles, is chemically changed into a gel, which is a semi-solid network. In a liquid media, the transition involves the hydrolysis and polymerization of precursors, usually metal alkoxides. The gel is created as a result of these reactions, which form a network of linked particles. Tetraethyl orthosilicate (TEOS) is the most widely used silica precursor in single-phase sol–gel coatings [19,24–27]. These coatings are valued for their elasticity, water-repellent properties and strong compatibility with glass, thanks to their similar chemical composition [19,28]. In recent years, additional sol–gel formulations for glass and ceramic materials have been developed and patented by academies and industries [27,28]; thus many products are currently available for purchase. However, there is a lack of literature regarding their long-term exposure or comparative tests with commonly used coatings.

This work focuses on the weathering of outdoor glass in unsheltered conditions (such as historic stained-glass windows and mosaic tiles), where deterioration is caused by exposure to temperature and humidity variations, solar radiation and the combined chemical and mechanical effects of rainwater runoff. Specifically, the research aims to

(i) Investigate the degradation of two types of traditional silicate glass (a soda-silicate glass, and a mixed-alkali glass rich in lead) when exposed outdoor in runoff conditions;

(ii) Test and evaluate the performance of consolidant and protective treatments on representative weathered glass substrates obtained at point (i). Two products were chosen among new commercial sol–gel options available to restorers and conservation operators. These were compared with the well-established acrylic coating Paraloid B72.

This was achieved in a controlled laboratory setting, where natural weathering was suitably replicated through an accelerated aging protocol that simulates outdoor corrosion by incorporating key factors such as rainfall composition and pH, reflecting past and current air pollution conditions, temperature and humidity cycles and UVA radiation from sunlight.

2. Materials and Methods

2.1. Glass

Two silicate glass sheets with different traditional compositions and different colors (blue and orange) were supplied by the "Orsoni" furnace (Venice, Italy), a manufacturer specialized in the production of traditional glass mosaic tiles. The chosen glasses are not exact mimics of specific glass productions; they were instead chosen to showcase the influence of different compositions on the corrosion patterns of glass when exposed outdoors. The choice of traditional glass composition represents an acceptable compromise between the use of real historical glass compositions and the need to avoid uncontrollable variables. The real historical glass composition would have introduced the possibility that the results could be sample-dependent, a circumstance that should be avoided in testing the coatings' behaviors. The modern stained-glass types were also chosen for the availability of massive quantities of homogeneous glass to be sampled and prepared for the numerous steps of the test [29].

The first glass type (Table 1) is a blue silicate glass with the addition of an alkali mixture (Na and K). A small amount of Ca is present as a stabilizer. Pb is present in a relatively large amount as a fluxing agent and to enhance chemical resistance and the refractive index [5–7]. There is also a significant concentration of antimony that was used in antiquity as an opacifier (%Sb > 1) or as a decolorizer (Sb around 0.5%) [30–32]. The blue colour is due to the presence of Co [33,34].

Table 1. Composition (wt%) of the two glass types. Data obtained through SEM/EDS by scanning the surface of the glass specimens; all areas were scanned at a magnification of 500× (average and related standard deviations are reported).

blue glass	**C**		**O**		**Na**		**Al**		**Si**		**Sb**		**Cl**		**K**		**Ca**		**Co**		**Pb**	
		±		±		±		±		±		±		±		±		±		±		±
	3.1	1.0	38.6	0.5	9.0	0.7	0.3	0.0	24.1	0.6	1.7	0.2	0.1	0.0	2.1	0.1	0.8	0.0	0.1	0.1	20.1	0.7
orange glass	**C**		**O**		**Na**		**Al**		**Si**		**S**		**Cl**		**K**		**F**		**Zn**		**Cd**	
		±		±		±		±		±		±		±		±		±		±		±
	1.2	0.6	41.3	0.2	18.9	0.2	0.1	0.0	27.6	0.7	0.3	0.0			0.1	0.0	0.5	0.4	9.6	0.5	0.3	0.1

The second glass type (Table 1) is an orange sodium silicate glass. Zn is added as a stabilizing agent, while Cd is responsible for the orange color [35].

The 0.7 cm thick glass plates were cut into roughly 2 × 2 cm specimens by hand. The area and weight of each specimen were measured prior to the experiments.

2.2. Protective Coatings

Two consolidant and protective products, belonging to the Siox-5 series produced by SILTEA (Padova, Italy), have been selected from new commercially available sol–gel formulations. Different Siox-5 products have been used in conservation projects in recent years [19,28,36,37]. Such coatings may represent a good solution for glass conservation due to their chemical characteristics; however long-term comparative testing against other common coatings has not yet been performed [37]. In this work, the performance of Siox-5

RE20C and Siox-5 RE39 was compared with that of Paraloid B72, an acrylic resin widely used in glass conservation [19] and serving as a benchmark.

Siox-5 RE20C is a highly concentrated consolidating agent, acting also as a water-repellent protectant. The product is a 40% alcohol solution containing nanostructured silica that has been functionalized with organically modified silicon alkoxides. It is commercially sold as a consolidant ideal for fragile weathered glass prone to surface flaking. Siox-5 RE20C is ready-to-use and can be applied to specimens either by spraying or brushing [19,38]. The product has been used in restoration projects, though there are no published results regarding its long-term performance.

Siox-5 RE39 is a liquid formulation consisting of a 20% alcohol solution of pre-cross-linked silica that is marketed as a pre-consolidant [36]. When the product is applied to the mineral matrix, it solidifies into a layer of amorphous inorganic silica, which is compatible with both silicate and carbonate substrates. Like Siox-5 RE20C, this product can be directly applied as it is by spraying or brushing.

Paraloid B72 is a copolymer of ethyl methacrylate and methyl acrylate. Its composition has changed over the years, with the 1978 formulation having a nominal composition of 70:30%. It has a glass transition temperature of 40°, a refractive index of 1.49 and, being thermoplastic, it is generally reversible. Paraloid may be sensitive to environmental conditions, primarily solar radiation, since UV rays may induce chemical changes that affect the efficacy of the coating [39]. For this reason, application of Paraloid resins is sometimes suggested for indoor applications [19,40]. The properties of the final coating are strongly dependent on the method of resin preparation, especially the choice and ratios of the solvent. Some commonly used solvents for Paraloid B72 include acetone, toluene, xylene, ethyl acetate and diacetone alcohol [39,41–43]. For glass protection, Paraloid B72 is generally employed in concentrations in the range of 2.5–7.5 wt%, ensuring a low-viscosity formulation that can penetrate degraded substrates. Here, Paraloid B72 resin pellets (AN.T.A.RES srl. San Lazzaro di Savena (BO), Italy) were dissolved in acetone to form a 3 wt% solution.

The surface of the glass specimens was cleaned with pure ethanol to remove any possible residues prior to coating application. A side for main analysis was selected, and all faces were mapped to scale in AgiSoft AutoCAD (version R.47.0.0 AutoCAD 2021, © 2020 Autodesk, Inc.) to determine total surface area. All the products were applied to the glass specimens using a brush, creating a clear and thin layer across the entire surface of the glass. The amount of product on the surface was estimated through gravimetry by comparing the weight of specimens before coating application and weight recorded after full coating drying. Results showed that the amount of product deposited on the specimens was in the range of 0.04–0.07 mg/cm^2 for Paraloid B72 and Siox-5 RE39, while values around 0.1 mg/cm^2 were found for Siox-5 RE20C.

2.3. Artificial Aging Protocol

The experiment was divided in two phases. In the first phase, named the “pre-aging phase”, bare glass specimens were subjected to rain exposure in runoff conditions, followed by temperature and humidity cycling in a climatic chamber. Through this phase, aged glass specimens are obtained, which can be used as “real” representative substrates for the application of protective coatings.

In the second phase of the study, named the “aging phase”, the artificial aging process is repeated to evaluate the performance of the coatings. In this phase, part of the specimens is also exposed to UVA light inside the climatic chamber to evaluate the sensitivity of coatings to this type of radiation.

The entire experimental design is summarized in Figure 1. Time labels indicating the pre-aging (p-t) and aging phases (a-t) are reported.

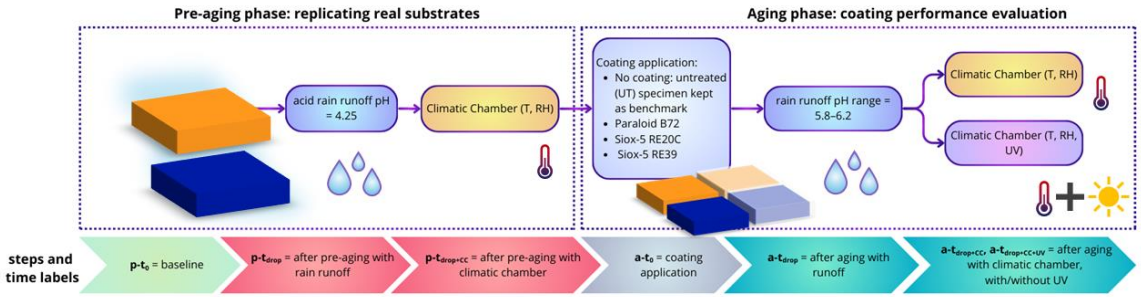

Figure 1. Graphical representation of the experimental design: p-t = pre-aging time; a-t = aging time. drop = rain dripping test; CC = climatic chamber; UT = untreated.

2.3.1. Rainwater Runoff

A customized dripping device was designed and perfected in previous studies [44,45]. The glass specimens were positioned on Teflon supports at an angle of 45°. A system of tubes and a peristaltic pump lets 4 synthetic rain droplets fall on the glass specimens with a flow rate of 57 cm^3/h and a drop fall height of about 2.5 cm.

The test was conducted intermittently, with one day of drying after 2 or 3 days of continuous rain dripping. This method simulates not only the rain runoff phase but also the onset of rain events and rain evaporation. This allows aggressive species to concentrate in the residual surface rain layer during the evaporation phase, with possible variations in surface pH; it also enables cycles of crystallization and dissolution of eventual weathering products.

During pauses, rain runoff samples were collected for analysis. The experiment is conducted for a total of 20 days of time of wetness (ToW).

Two different rain formulations were used in the runoff test, depending on the experiment's phase.

The pre-aging phase is aimed at replicating the degradation process that historical glass underwent in the past. Therefore, an acid rain solution based on the composition of wet acid depositions sampled in Bologna (Italy) around two decades ago was used [44,46,47]. The acid rain has a pH of 4.25 and contains the following concentrations of ions: SO_4^{-2} 1.90 mg L^{-1}, NO_3^- 4.64 mg L^{-1}, Cl^- 1.27 mg L^{-1}, CH_3COO^- 0.23 mg L^{-1}, $HCOO^-$ 0.05 mg L^{-1}, NH_4^+ 1.06 mg L^{-1}, Na^+ 0.53 mg L^{-1} and Ca^{2+} 0.34 mg L^{-1}.

In the aging phase, which is aimed at simulating current environmental attack on glass and conservative treatments, a rain solution representative of current trends in air pollutants in the Mediterranean region was used. Here, a reduction in SO_x and NO_x concentrations, coupled with an increase in alkaline species, is leading to an increase in rain pH [48]. This rain therefore has a pH falling between 5.8 and 6.2 and contains the following concentrations of ions: SO_4^{2-} 1.58 mg L^{-1}, NO_3^- 1.56 mg L^{-1}, Cl^- 3.39 mg L^{-1}, NH_4^+ 0.99 mg L^{-1}, Na^+ 1.03 mg L^{-1}, Ca^{2+} 0.55 mg L^{-1} (0.23 of which added as carbonate) and Mg^{2+} 0.24 mg L^{-1}.

Both synthetic rains were prepared using analytical-grade reagents and deionized water.

2.3.2. Climatic Chamber

To replicate the effects of natural weathering due to variations in temperature (T), relative humidity (RH) and UVA exposure, a tailored aging cycle was designed in a climatic chamber (Climacell 111, MMM Medcenter Einrichtungen GmbH, München, Germany). The cycle lasts 16 h 30 min and includes two transition ramps connecting two stable conditions, each maintained for 6 h 30 min: the first at T = 10 °C and RH = 90% (to mimic winter

nights), and the second at T = 50 °C, RH = 30% and UVA light (300–400 nm; 4 mW/cm^2) (to mimic summer days and average UVA at midday sunlight in southern Europe). The cycle was repeated continuously for three weeks, the parameters were chosen to reproduce condensation/evaporation cycles. In fact, a surface is generally considered to be wet by atmospheric moisture at RH > 80% (at temperatures above 0 °C) [49]. During the pre-aging phase, none of the specimens (all uncoated) were exposed to UV light. In the subsequent aging phase, only half of the specimens (both coated and uncoated) were exposed to UVA radiation in order to evaluate its effect.

2.4. Characterization

2.4.1. Surface

Before and after each step of the experiment, microscopic alterations in the glass specimens' surfaces were monitored through scanning electron microscopy. Additionally, elemental analysis was carried out to identify patterns in elemental composition changes. Glass specimens were investigated through the combined use of scanning electron microscopy (SEM) with a Zeiss EP EVO 50 (Carl Zeiss AG, Oberkochen, Germany) in variable-pressure mode (100 VP) and energy-dispersive X-ray spectrometry (EDS) with a INCA X-act Penta FET® Precision microprobe by Oxford Instruments (Tubney, United Kingdom). The accelerating voltage used for analyses was 20 kV.

A portable 3NH-YS3060 VIS spectrophotometer (3nh, Zengcheng District, Guangzhou, P.R. China) was employed to measure the color variations on the surface of each glass specimen, sampling at least two different points. The following parameters were set: Illuminant/Observer: D65/10°, Geometry: d/8, specular component included, 8 mm aperture and color measurements performed in the CIEL*a*b* system. In the field of cultural heritage, color changes are generally considered negligible when $\Delta E^* < 3$, and acceptable when $\Delta E^* \leq 5$ [50] where ΔE^* corresponds to the Euclidean distance between the chromatic coordinates: $\Delta E^* = (\Delta L^2 + \Delta a^2 + \Delta b^2)^{1/2}$.

During the aging phase, coating alterations were monitored through Attenuated Total Reflection Fourier Transform Infrared (ATR-FTIR). Measurements of the glass specimens were performed using the Spotlight 200i FT-IR Microscopy System with Spectrum 3 (Perten, a PerkinElmer Company, Springfield, IL, USA), equipped with a thermal source (Globar) and a deuterated triglycine sulphate (DTGS). The single-reflection ATR accessory by PIKE Technologies (Madison, WI, USA) with a diamond Internal Reflection Element (IRE) was used. Measurements were acquired with a spectral resolution of 2 cm^{-1} in the spectral range of 600–4000 cm^{-1} by averaging 64 scans. To improve clarity and minimize noise, the spectra were corrected for the baseline and atmospheric contribution. All spectra were normalized to the signal of the most intense band.

2.4.2. Runoff Solution

The runoff solution from the dripping test was periodically collected and analyzed to identify the release of modifier ions and silica dissolution phenomenon.

The total volume and pH of the solution were measured; 50 mL of solution was sampled in HDPE bottles. Samples were acidified to a pH < 2 using suprapur HNO_3 65% and stored at 4 °C [44,46].

Concentration of Na, K and Si were analyzed using microwave plasma atomic emission spectroscopy (MP-AES Agilent 4210). Pb concentration was measured only for blue glass specimens. The same elements were also analyzed in the rain before the runoff occurred (blank). For the measurement of Na and K concentrations, which are easily ionizable elements, 50 µL of an ionization suppressant (CsCl solution, 0.83 M in ultrapure water) was added to 5 mL of sample to improve the quality of the analysis.

Results were subtracted for the amount of analytes already present in the rain itself. Then, the cumulative mass release of each element was calculated, normalized by the area of glass exposed to the rain droplets.

3. Results and Discussion

The results are presented in two sections: the first concerns the pre-aging phase of the glass specimens, and the second the ageing phase of the specimens treated with coatings.

3.1. Pre-Aging Phase: Glass Weathering

The physical and chemical weathering of glass exposed to rain runoff in unsheltered conditions was investigated during the pre-aging phase. This phase was also effective in producing specimens representative of environmentally degraded glass for the subsequent phase of coating evaluation.

3.1.1. Surface Characterization

During the artificial aging process, the glass specimens showed color changes as a consequence of the physical and chemical alterations produced by the simulated environmental attack. Color differences were calculated between the initial glass color (measured at p-t_0) and the two pre-aging steps (p-t_{drop} and p-$t_{drop+CC}$). Total color variation ΔE* caused by pre-aging is represented in Figure 2, panel a.

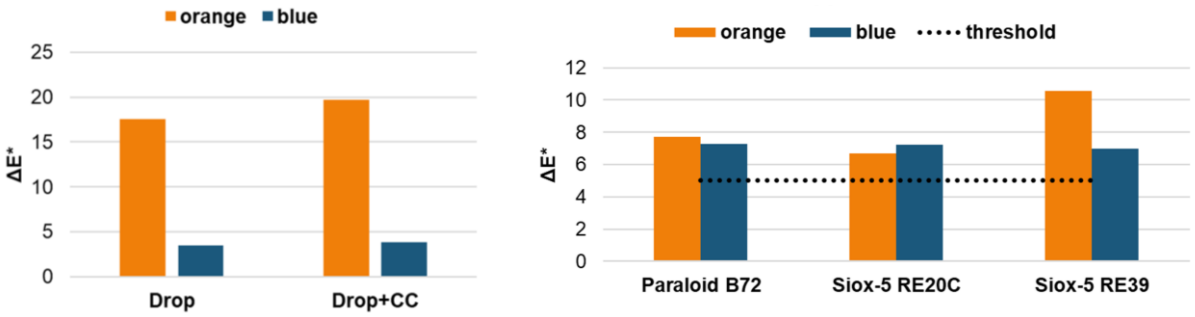

(**a**) (**b**)

Figure 2. (**a**) Total chromatic variation (ΔE*) exhibited by glass specimens during the pre-aging phase; (**b**) total chromatic variation caused by the application of coatings on the pre-aged glass specimens.

Overall, the chromatic variation was larger in the orange specimens than in the blue ones. The orange glass underwent the greatest color change, showing a total ΔE* much higher than 5, which is the limit considered acceptable in the field of cultural heritage: ΔE* = 18. In the orange glass, the color variation was given by a major increase in the L* variable (lightness), which indicates surface bleaching, and a decrease in saturation (a simultaneous decrease in both a* and b*) (Figure S1), Whereas in the blue specimens, where color variation was more contained, a decrease in L* was observed, along with a slight decrease in saturation (Figure S1). The trend observed is coherent with the physical state of the surface. In particular, the increase in L* can be related to the formation of surface inhomogeneities [51,52], which differed between the two substrates, being more pronounced for the orange glass, as highlighted by SEM results.

The SEM images (Figure 3), in fact, show significant differences in surface degradation between the blue and the orange glass specimens. After 10 days of ToW, the orange specimens had already begun to exhibit signs of crizzling, with the formation of surface cracks that can lead to the peeling of the outer layer of the glass. Disruption of the surface layer was very evident at the end of the pre-aging phase. During the drying phases of the tests, the hydrated silica gel layer, formed by alkali leaching in contact with synthetic

rain, tends to reach thermodynamic equilibrium with the environment [10]. Glasses with a composition particularly poor in CaO are more susceptible to crizzling [53,54]. The exact quantities of CaO needed to stabilize glass vary depending on the composition of other elements present in the glass besides SiO_2. Nevertheless, an amount of Ca on the order of 4% is typically needed [55]. CaO was present in the blue glass along with relevant amounts of Pb, but not in the orange one (Table 1). Thus, it is plausible to attribute the resistance to crizzling of the blue specimens to the stabilizing action of Ca and Pb.

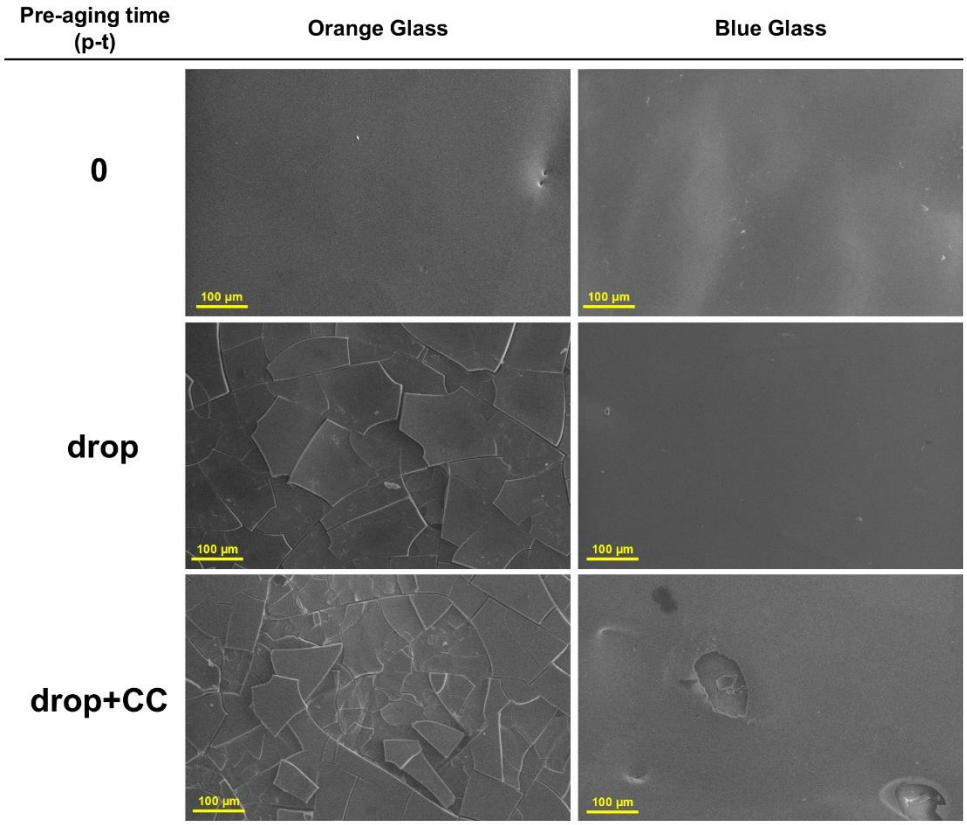

Figure 3. Secondary electron images of the glass surface during the pre-aging phase.

EDS analyses were carried out on areas at 500× magnification. The results were obtained by averaging the wt% values of the elements detected in comparable areas according to sample type and aging time.

Table 2 shows elemental results collected at different pre-aging times. In the orange glass, a relevant decrease in Na was observed. Alongside this, an increase in the weight % of O may be attributed to the formation of a hydrated layer, while a small apparent increase in the relative amounts of Si may be due to the depletion of alkali. These trends are typically observed in crizzled glass [55]. Zn wt% also appears to have diminished. A similar pattern was observed in the blue glass, which exhibited a decrease in modifier ions (Na and K) and an increase in O; here, Si wt% remained stable. Again, these results can be attributed to leaching of alkali modifier ions and formation of silanol bonds [10].

Table 2. Elemental composition (wt%) of the surface of the glass specimens during pre-aging. Data was obtained by averaging areas of comparable size at 500× magnification (average and related standard deviations are reported).

	pre-aging time (p-t)	C		O		Na		Al		Si		S		Cl		K		F		Zn		Cd	
			±		±		±		±		±		±		±		±		±		±		±
orange glass	0	1.2	0.6	41.3	0.2	18.9	0.2	0.1	0.0	27.6	0.7	0.3	0.0			0.1	0.0	0.5	0.4	9.6	0.5	0.3	0.1
	Drop (ToW 10d)	3.0	0.6	49.8	0.7	2.0	0.4	0.2	0.0	36.8	0.9	0.4	0.0							7.5	0.6	0.4	0.1
	Drop (ToW 20d)	3.0	3.7	50.7	2.3	2.8	2.9	0.2	0.1	33.6	2.1	0.4	0.0	0.2	0.1	0.0	0.1	1.0	1.5	7.6	1.1	0.3	0.1
	Drop+CC	2.1	1.0	53.4	0.9	4.7	1.5	0.2	0.0	31.1	1.6	0.3	0.0	0.0	0.0	0.0	0.0	0.4	0.0	7.5	0.7	0.4	0.1
	pre-aging time (p-t)	**C**		**O**		**Na**		**Al**		**Si**		**Sb**		**Cl**		**K**		**Ca**		**Co**		**Pb**	
			±		±		±		±		±		±		±		±		±		±		±
blue glass	0	3.1	1.0	38.6	0.5	9.0	0.7	0.3	0.0	24.1	0.6	1.7	0.2	0.1	0.0	2.1	0.1	0.8	0.0	0.1	0.1	20.1	0.7
	Drop (ToW 10d)	2.6		48.6	0.5	1.9	0.2	0.3	0.0	25.5	0.3	1.9	0.1	0.2	0.1	1.0	0.1	0.7	0.0	0.1	0.1	17.2	0.2
	Drop (ToW 20d)	4.9	2.7	45.5	1.8	2.2	1.3	0.3	0.0	26.0	1.4	2.0	0.1	0.2	0.1	1.0	0.3	0.8	0.0	0.1	0.1	17.9	1.5
	Drop+CC	2.5	0.8	47.4	2.4	3.2	1.3	0.3	0.0	25.1	0.6	1.9	0.1	0.2	0.0	1.1	0.5	0.7	0.0	0.0	0.1	17.6	1.5

Subsequent to thermo-hygrometric aging, elemental data does not appear significantly different.

As can be seen from Figure 4 and the corresponding elemental data (Table 3), salt deposits were observed on the surface of the glass specimens, especially in areas where the wash-off action of the artificial rain droplets was weaker, such as the borders of the surface. On the orange specimens, fluoride salts were observed, which are likely recrystallizations of NaF, a salt commonly used as an opacifier in glass making [56]. A few carbon-rich salt deposits (with C weight % ranging roughly from 10 to 40%) were also observed on both the orange and blue glass. These could be carbonate salts formed by interaction of the leached alkali and bicarbonate ions from the atmosphere, but the formation of organic salts (particularly sodium acetates and formates) is also possible [57], given the composition of the artificial rain, which includes acetic and formic acid. Scarce nitrate salts could also be present, as shown in Supplementary Material (Figure S2).

Table 3. Results of EDS analysis carried out in points shown in Figure 4. Data is reported as weight%.

	C		O		F		Na		Al		Si		S		Cl		K		Zn		Cd	
		±		±		±		±		±		±		±		±		±		±		±
1	1.1	0.3	12.4	0.2	44.9	0.3	25.2	0.2	0.1	0.0	13.0	0.1	0.1	0.0					3.2	0.1	0.1	0.1
2			12.8	0.2	45.2	0.2	24.9	0.2	0.1	0.0	13.4	0.1	0.1	0.0	0.0	0.0			3.4	0.1	0.2	0.1
3			38.9	0.6	11.7	0.7	17.9	0.4	0.2	0.1	18.6	0.3	7.5	0.2	0.4	0.1			4.4	0.3	0.2	0.2
4	15.0	0.9	48.8	0.6			3.2	0.1	0.2	0.0	26.3	0.3	0.3	0.0	0.5	0.0	0.1	0.0	5.5	0.2	0.3	0.1
5	10.4	1.4	51.3	0.9			2.5	0.2	0.1	0.1	28.9	0.6	0.2	0.1			0.1	0.1	6.1	0.3	0.5	0.2
6	11.0	1.3	50.1	0.9	0.6	0.4	6.1	0.3	0.2	0.1	23.6	0.5	0.2	0.1	0.1	0.1			7.7	0.4	0.3	0.1
7	29.1	1.4	40.7	1.1			2.3	0.3			15.6	0.5	0.2	0.1					11.8	0.7	0.3	0.2
	C		**O**		**Ca**		**Na**		**Al**		**Si**				**Cl**		**K**		**Sb**		**Pb**	
		±		±		±		±		±		±				±		±		±		±
8	32.7	1.3	37.5	0.8	1.0	0.1	3.0	0.1	0.2	0.0	14.5	0.3			0.3	0.1	0.5	0.1	1.3	0.2	9.2	0.3

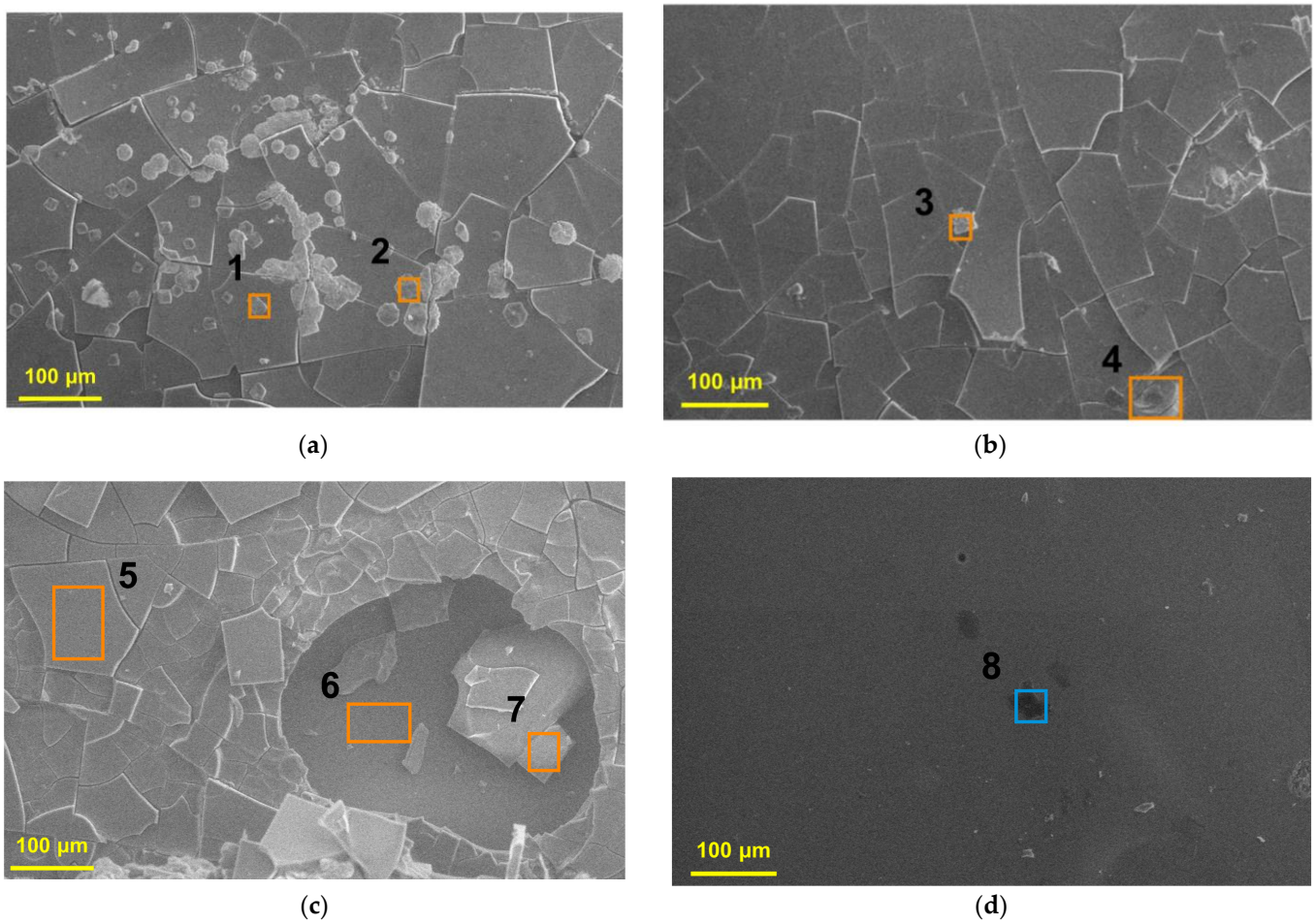

Figure 4. Secondary electron images of areas showing salt deposits, along with areas where EDS analysis was performed. (**a**) Orange glass at p-t_{drop} showing recrystallizations of NaF; (**b**) orange glass at p-t_{drop}; (**c**) orange glass at p-$t_{drop+CC}$; (**d**) blue glass at p-$t_{drop+CC}$. Numbers indicate the points of the EDS analyses whose results are shown in Table 3.

3.1.2. Runoff Solution

Because of its important role in glass corrosion, the pH of the runoff solution was monitored. It rose by 0.07 ± 0.04 after renewals every 2–3 days of ToW. This increase in pH is attributed to the continuous leaching of alkali metals; the relatively modest increase may be due to the significant dilution of the leaching solution.

The results of element release revealed that Si, a major component of the glass matrix, was not significantly leached across all runoff test (always lower than the limit of detection, LoD = 15 ppb). Si is known to be soluble under alkaline conditions, but under acidic exposure (e.g., acidic rain), a silica-rich layer forms, limiting the leaching of Si while promoting the release of modifying ions (e.g., K, Na, Pb) that are more soluble at pH < 9.

By examining surface elemental data (Table 2), it is evident that both glass types have undergone some Na leaching. However, the concentration of Na detected in the runoff solution was found not to be significantly different from that of the artificial rain; thus it could not be reliably quantified. This is probably due to the dilution effect caused by the relatively low amount of sodium released into a large volume of rainwater, which already contains a non-negligible amount of Na.

K release, on the other hand, can be reliably quantified (Figure 5).

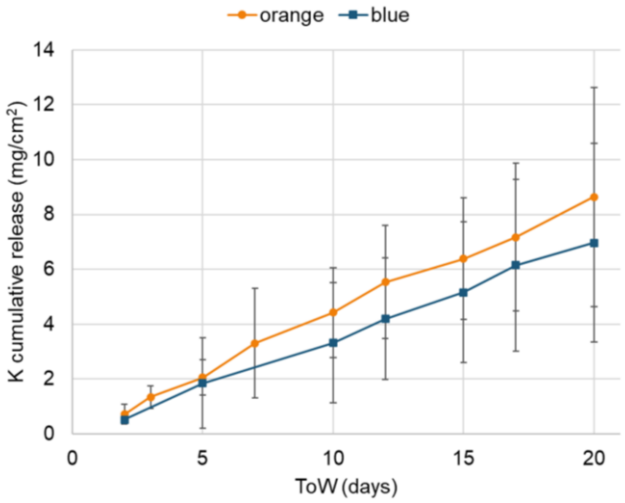

Figure 5. K release from orange and blue glass specimens during the pre-aging phase. ToW = Time of Wetness. Error bars represent standard deviation calculated among replicates.

Notably, despite being present in low quantities in both glass types (especially the orange one), the release of K appears to be quite high, particularly in the orange specimens (though the difference was not found to be statistically significant). Comparing the quantities of released K across glass compositions (Table 1), it seems that orange glass releases K more easily compared to the blue one. This might be attributed to the presence of ions with a strong stabilizing effect in the blue glass (Ca and Pb), which inhibits mobility within the glass network [3,5,58]. This leads to better physical and chemical resistance, as is proven by the better state of conservation of the blue glass' surface compared to the orange glass' one (Figure 3).

Pb release was monitored in the blue samples. Pb concentration predominantly remained below the Limit of Quantification (LOQ) of 8 ppb. Notably, during the first few days of testing (approximately 10 ToW), the analysis of runoff solutions revealed the presence of traces of Pb. However, in the remaining days of pre-aging, Pb was no longer detectable (limit of detection, LOD = 5 ppb), indicating that surface Pb is slightly leached during the initial stages of degradation, after which the leaching appears to slow down or cease.

3.2. Aging Phase: Coating Evaluation

3.2.1. Surface Characterization

Color variation caused by coatings on glass was measured by comparing specimens at the end of pre-aging (p-$t_{drop+CC}$) and at the moment of treatment application (a-t_0). ΔE^* is reported in Figure 2, panel b. On both glass types, all coatings caused a total chromatic variation of 1 to 6 units above the acceptable threshold for cultural heritage ($\Delta E^* > 5$). In all instances, the application of a smooth transparent layer on inhomogeneous surfaces lead to a decrease in lightness (L*) [51], as can be evidenced from graphs reported in Figure S3. This is particularly noticeable on the orange glass, which, after pre-aging, had a rougher, crizzled texture compared to the blue one (Figure 3).

Throughout the aging phase, the glass surface was affected by further color alterations. Differences in color variation were observed between treated and untreated specimens, as well as among the different protective coatings (Figure 6).

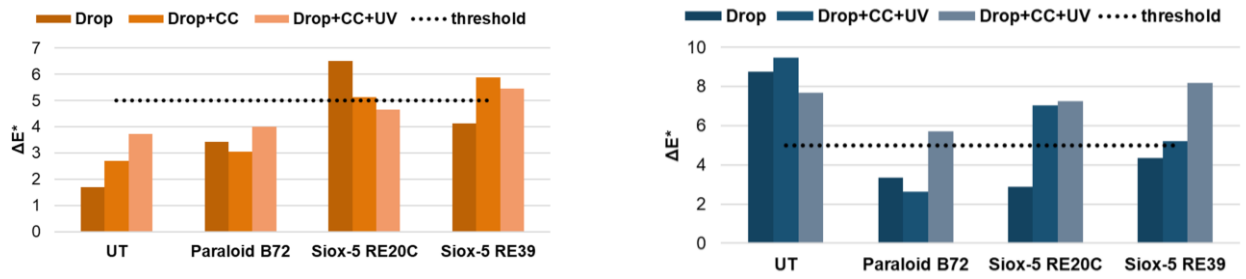

Figure 6. Total chromatic variation (ΔE*) in the untreated (UT) and coated glass specimens during the aging phase: (**a**) orange glass and (**b**) blue glass.

All coated specimens showed an increase in L* (Figures S4 and S5), related to the increase in physical inhomogeneities on the surfaces, coherent with SEM observations discussed in the later paragraphs. In the case of the two Siox-5 coatings, this increase in L* contributed to reaching or exceeding the acceptable threshold of ΔE* = 5.

On the other hand, Paraloid-coated specimens generally showed acceptable chromatic changes (ΔE* < 5). However, blue specimens exposed to UVA radiation exhibited an increase in the b* variable (Figure S5), leading to a ΔE* slightly above 5. This yellowing tendency could be masked by the color of the substrate in the case of orange specimens.

By comparing the concentration values of the major elements between untreated (UT) and coated glass specimens (Table 4), it is evident that these vary depending on the protective coating applied. For Paraloid B-72, both for the orange and blue specimens, a high concentration of C is observed, accompanied by a corresponding decrease in all elements. This is consistent with the presence of a protective layer on the glass surface and the organic nature of the coating, which is mainly composed of C and O. For Siox-5 RE20C, an increase in the concentration of Si, C and O is observed, with a corresponding decrease in K, Na and, for blue specimens, Pb. Similar trends were observed for Siox-5 RE39. Again, these results are consistent with the chemical composition of the coatings, which is mainly made up of Si, O and C.

Figure 7 shows the morphology of the surface of the orange glass specimens during aging. On this substrate, the protective coating that shows the best adhesion and durability over time seems to be Siox-5 RE39, whereas Paraloid B-72 exhibits the typical crizzling phenomenon. The sol–gel coating Siox-5 RE20C demonstrated poor adhesion, with evident detachment.

From the SEM images of the blue specimens exposed to runoff (Figure 8), it can be observed that the protective coating showing the lowest adhesion to the glass substrate is Siox-5 RE20C, as in the case of the orange glass (Figure 7). As mentioned in Section 2.2, this coating is recommended as a consolidant for severely flaked and porous glasses [19], and the blue specimens, after the pre-aging process, did not exhibit significant signs of degradation. Therefore, its penetration and adhesion may be poorer compared to the other two coatings. Detachment is also demonstrated by a relative increase in the Pb signal in EDS analysis, which is due to a decrease in the shielding effect of the coating (Table 4). The other sol–gel coating (Siox-5 RE39) also showed some signs of detachment, though to a lesser extent.

Table 4. Elemental composition (wt%) of coated glass specimens through the aging phase. Data was obtained by averaging areas of comparable size at 500× magnification.

	Treatment	Aging Time (a-t)	C	±	O	±	Na	±	Al	±	Si	±	S	±	Cl	±	K	±	F	±	Zn	±	Cd	±
Orange Glass	UT	0	2.1	1.0	53.4	0.9	4.7	1.5	0.2	0.0	31.1	1.6	0.3	0.0	0.0	0.0	0.0	0.0	0.4	0.0	7.5	0.7	0.4	0.1
		Drop	3.5	1.9	50.9	0.8	2.7	2.3	0.2	0.0	32.3	2.0	0.3	0.0	0.1	0.1	0.3	0.2	0.9	1.4	8.3	1.4	0.3	0.1
		Drop+CC	1.8	2.5	51.6	0.4	3.2	0.1	0.2	0.0	33.6	1.2	0.3	0.1	0.1	0.1	0.4	0.0	0.4	0.6	8.3	1.7	0.3	0.1
		Drop+CC+UV	3.5	4.6	51.9	2.6	4.4	0.4	0.2	0.1	30.6	1.5	0.3	0.1	0.2	0.1	0.1	0.1	0.5	0.5	7.6	0.6	0.2	0.2
	Paraloid B72	0	47.7	0.4	33.6	0.3	1.1	0.1	0.1	0.0	13.5	0.1	0.1	0.0							3.8	0.1	0.1	0.1
		Drop	44.3	4.6	33.9	2.3	1.4	0.8	0.1	0.0	16.5	1.7	0.2	0.0	0.1	0.1	0.1	0.1	0.2	0.1	3.0	0.6	0.2	0.1
		Drop+CC	45.7	9.3	33.1	3.4	1.4	0.7	0.1	0.1	17.1	4.1	0.1	0.0	0.0	0.0	0.0	0.0	0.0	0.0	2.0	1.0	0.2	0.1
		Drop+CC+UV	34.8	12.0	39.0	5.6	1.9	0.7	0.1	0.0	20.7	5.7	0.2	0.0	0.0	0.0	0.1	0.1	0.1	0.1	2.8	0.8	0.2	0.1
	Siox-5 RE20C	0	16.4	0.7	44.6	0.4	0.9	0.1	0.1	0.0	35.1	0.3	0.2	0.0							2.5	0.1	0.2	0.1
		Drop	17.0	2.6	44.0	1.2	1.1	0.6	0.1	0.1	33.8	0.7	0.2	0.1	0.1	0.1	0.1	0.1			3.4	0.6	0.1	0.2
		Drop+CC	12.6	9.0	45.8	4.1	1.7	1.6	0.1	0.1	36.0	1.4	0.2	0.1	0.1	0.0	0.1	0.0	0.0	0.0	3.1	3.0	0.2	0.1
		Drop+CC+UV	9.9	8.7	46.6	4.5	2.1	1.7	0.2	0.0	37.8	0.7	0.2	0.1	0.1	0.1	0.1	0.1			2.8	2.1	0.2	0.2
	Siox-5 RE39	0	0.9	0.9	54.5	0.6	3.3	0.2	0.1	0.1	34.7	0.4	0.3	0.1							5.8	0.3	0.3	0.1
		Drop	6.7	2.6	50.5	0.8	1.9	1.3	0.1	0.0	33.8	2.1	0.2	0.0	0.1	0.1	0.1	0.1	0.0	0.0	5.9	0.5	0.2	0.2
		Drop+CC	1.0	1.7	53.1	1.1	2.9	1.0	0.2	0.1	37.0	2.1	0.2	0.1	0.0	0.0	0.3	0.1	0.4	0.3	4.5	0.3	0.2	0.1
		Drop+CC+UV	3.9	0.3	51.9	0.6	3.7	1.3	0.2	0.0	34.0	1.0	0.2	0.1	0.1	0.1	0.2	0.1	0.3	0.4	5.0	0.5	0.4	0.1

	Treatment	Aging time (a-t)	C	±	O	±	Na	±	Al	±	Si	±	Sb	±	Cl	±	K	±	Ca	±	Co	±	Pb	±
Blue Glass	UT	0	3.1	1.0	38.6	0.5	9.0	0.7	0.3	0.0	24.1	0.6	1.7	0.2	0.1	0.0	2.1	0.1	0.8	0.0	0.1	0.1	20.1	0.7
		Drop	3.4	3.2	47.2	0.9	1.1	0.5	0.3	0.1	26.9	0.8	2.1	0.2	0.1	0.1	0.6	0.1	0.8	0.0	0.1	0.1	17.5	1.0
		Drop+CC	5.2	1.3	47.3	0.8	2.0	0.1	0.3	0.0	25.8	0.4	2.0	0.2	0.2	0.1	0.7	0.1	0.7	0.1			15.8	0.4
		Drop+CC+UV	3.3	4.7	47.3	1.6	2.3	0.5	0.3	0.1	26.0	1.7	2.0	0.3	0.3	0.1	0.7	0.2	0.8	0.1	0.2	0.0	16.8	1.1
	Paraloid B72	0	41.6	1.1	32.4	0.7	1.1	0.1	0.2	0.0	13.8	0.3	1.2	0.2	0.1	0.0	0.4	0.0	0.5	0.1			8.7	0.3
		Drop	42.0	7.8	31.1	4.6	0.3	0.1	0.2	0.0	15.0	1.9	1.1	0.1	0.1	0.0	0.3	0.1	0.6	0.1	0.0	0.0	9.2	1.1
		Drop+CC	51.4	9.4	27.3	4.3	0.9	0.4	0.1	0.0	11.5	2.6	0.8	0.1	0.1	0.1	0.4	0.2	0.4	0.1	0.0	0.0	7.1	1.9
		Drop+CC+UV	51.5	3.8	27.5	1.5	0.9	0.2	0.2	0.0	11.3	1.2	0.9	0.0	0.1	0.0	0.3	0.1	0.5	0.1	0.0	0.0	6.9	0.9
	Siox-5 RE20C	0	17.2	3.0	44.4	1.7	0.5	0.1			34.9	1.3	0.3	0.2	0.1	0.1	0.2	0.1	0.1	0.1			2.0	0.3
		Drop	15.9	1.4	42.7	0.0	0.3	0.1	0.1	0.0	35.2	0.7	0.6	0.2	0.1	0.0	0.1	0.0	0.2	0.0			4.7	0.5
		Drop+CC	16.0	0.5	42.5	0.7	0.8	0.2	0.2	0.0	33.0	1.6	0.8	0.1	0.1	0.0	0.3	0.1	0.3	0.1	0.0	0.0	6.2	1.7
		Drop+CC+UV	14.7	0.9	42.2	0.8	0.9	0.1	0.2	0.1	32.2	1.9	1.1	0.3	0.1	0.0	0.4	0.0	0.3	0.0	0.1	0.1	7.7	1.6
	Siox-5 RE39	0	3.5	0.9	52.4	0.5	2.0	0.1	0.2	0.0	28.3	0.3	1.4	0.1	0.2	0.0	0.5	0.0	0.5	0.1			11.1	0.2
		Drop	8.1	1.4	48.4	1.3	0.8	0.3	0.3	0.0	27.9	1.1	1.3	0.2	0.1	0.0	0.4	0.2	0.5	0.1	0.0	0.0	12.1	2.2
		Drop+CC	7.1	2.5	48.6	1.5	1.9	0.1	0.3	0.0	27.9	1.3	1.6	0.4	0.2	0.1	0.5	0.2	0.5	0.1	0.0	0.0	11.5	3.2
		Drop+CC+UV	5.0	3.2	50.0	1.2	2.0	0.3	0.2	0.0	29.8	1.5	1.1	0.2	0.2	0.1	0.5	0.2	0.5	0.1	0.1	0.1	10.6	1.7

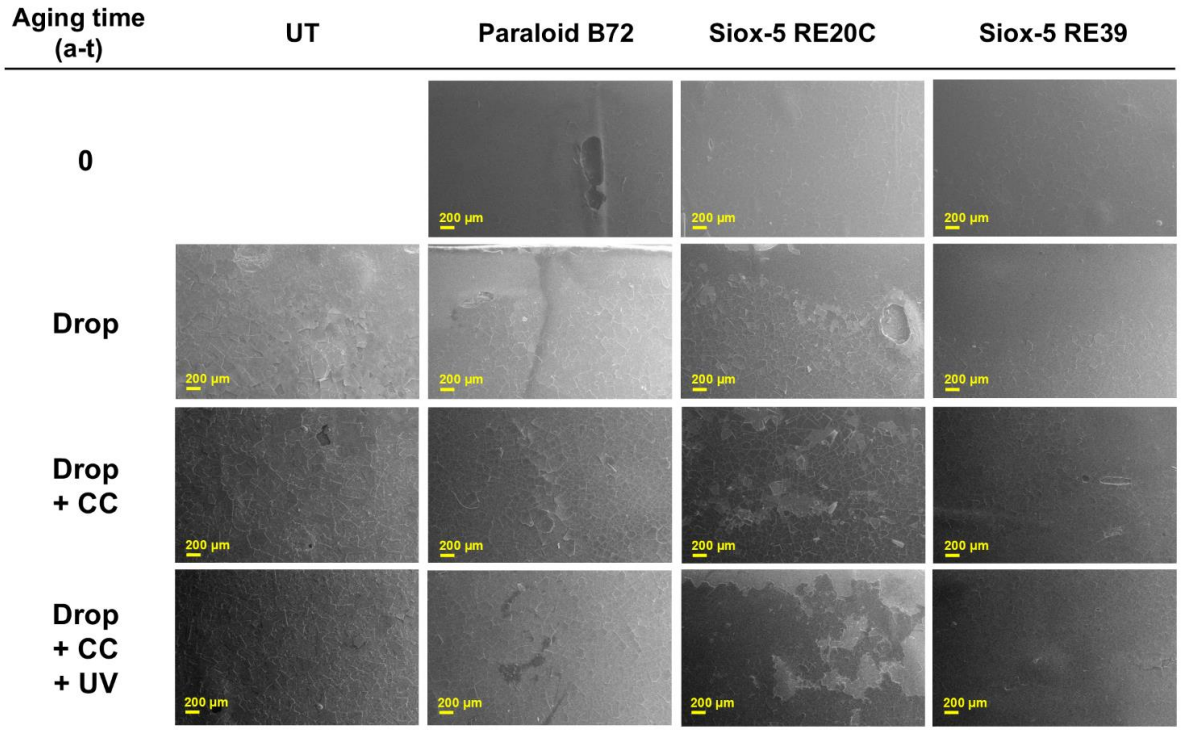

Figure 7. Secondary electron images of the orange glass specimens during the aging phase. UT = untreated glass.

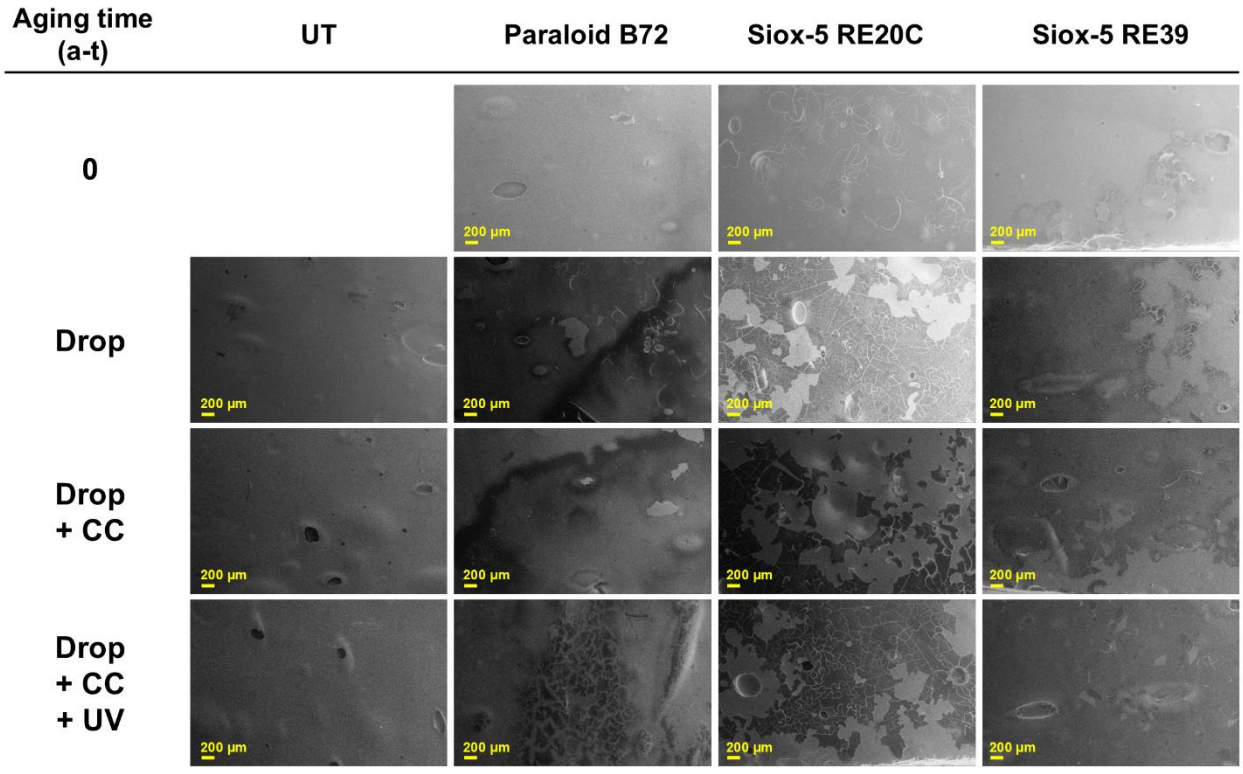

Figure 8. Secondary electron images of the blue glass specimens during the aging phase. UT = uncoated glass.

The glass specimens were also analyzed using ATR-FTIR spectroscopy. This technique enables the presence of protective coatings on glass substrates to be evaluated, as well as their potential degradation, by studying the variations in characteristic bands at different stages of accelerated aging.

The specimens were monitored under four conditions: at the initial aging time (a-t_0), after exposure to artificial rain (a-t_{drop}), and following treatment in the CC without (a-$t_{drop+CC}$) or with UV radiation (a-$t_{drop+CC+UV}$).

Figure 9 compares the ATR-FTIR spectra collected for both blue (panel a) and orange uncoated glasses (panel b) throughout the aging phase. The bands around 789 and 1030 cm^{-1} refer, respectively, to bending and stretching vibrations of the Si-O-Si group in the presence of Na_2O in both types of glasses treated under all experimental conditions [59–61].

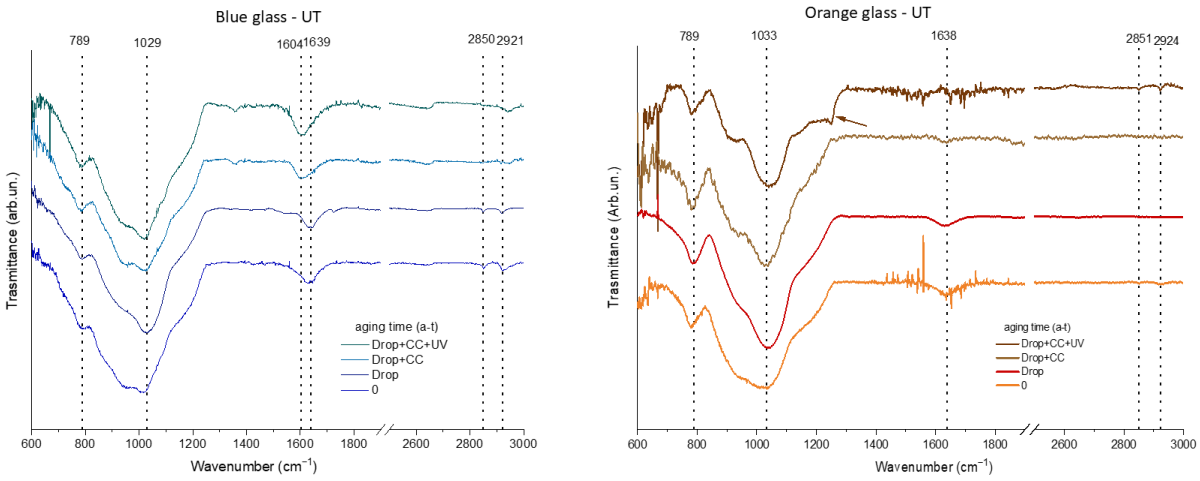

(**a**) (**b**)

Figure 9. ATR FTIR spectra of uncoated (UT) glass at different aging times: (**a**) blue glass and (**b**) orange glass.

The bands at 2854 and 2922 cm^{-1}, attributed to C-H stretching vibrations [62] and likely occurring due to organic contaminants or salts on the surface, disappear after the CC and CC+UV treatments.

The band around 1640 cm^{-1} corresponds to O-H bending. In panel a, following the CC and CC+UV treatments of blue glasses, this band shifts down to 1604 cm^{-1}, which could be due to water adsorption causing changes in the local structure of the silanol groups in the glass. On the other hand, in panel b, this band disappears after T and RH cycling in the climatic chamber (CC) with or without UV, likely indicating desorption of molecular water [61,63,64].

In the orange glass, in addition, the CC+UV spectrum shows a shoulder around 1250 cm^{-1}, as indicated by the arrow in Figure 9 (panel b), attributed to Si–O–Si stretching. This spectral evolution suggests that the CC and UV treatments induce a drying effect in the glass, with the disappearance of the O–H stretching band being consistent with the condensation of silanol (Si–OH) groups into siloxane (Si–O–Si) bonds. The presence of the shoulder at 1250 cm^{-1} may also indicate the onset of structural rearrangements that could promote corrosion in the orange glass.

Such behavior aligns with observations reported by Lynch et al., where similar condensation and drying phenomena at elevated temperatures led to cracking in treated glasses [65].

These results are also consistent with the SEM findings described above, where it was observed that the orange soda-silicate glass is more susceptible to crizzling.

Figure 10 compares the ATR-FTIR spectra collected for both blue (panel a) and orange glasses (panel b) coated with Paraloid B-72 in the aging phase. The main absorption bands of Paraloid B72 appear at 1140 (C–C=O–O stretching modes), 1387 (CH_3 symmetric bending

modes), 1445 (CH_3 asymmetric bending mode), 1725 (ester carbonyl group stretching mode), 2954 and 2922 (C–H stretching modes) cm^{-1} [66,67]. In the case of blue glass, which presents a more uniform surface and no signs of crazing, it is possible to detect the signals with less intense bands, such as those at 860 (C–H rocking modes) and 1239 (C–C=O–O stretching modes) cm^{-1}.

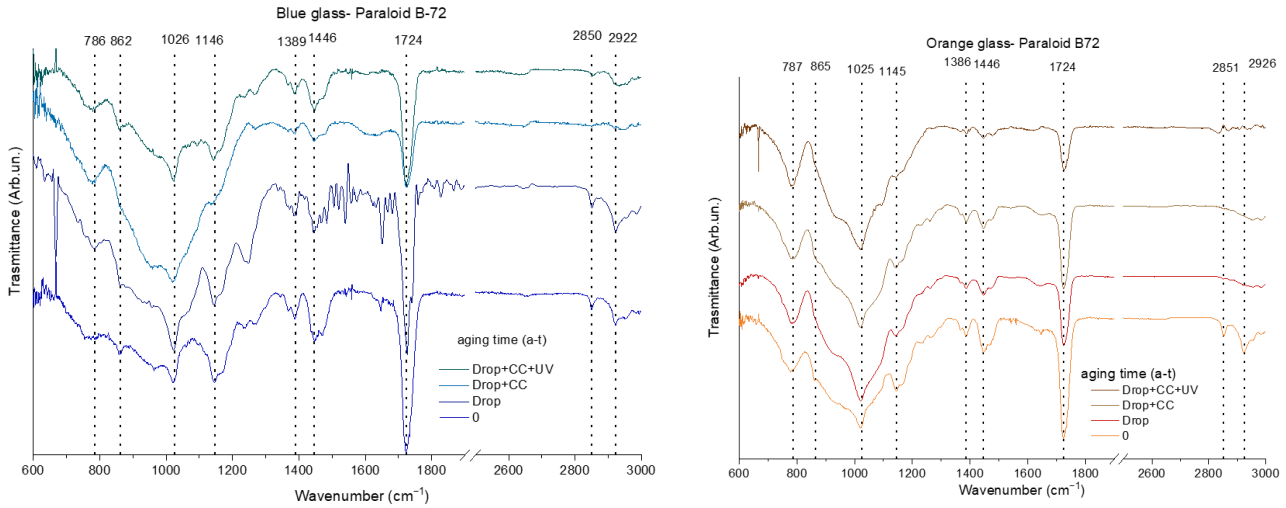

(**a**) (**b**)

Figure 10. ATR FTIR spectra of glass coated with Paraloid B72 at different aging times: (**a**) blue glass and (**b**) orange glass.

As shown in panel a, there are no significant differences between the spectra of Paraloid B-72 before and after rain exposure, suggesting that the dripping procedure did not alter the protective coating on the blue glass. However, after CC and CC+UV aging, the bands at 2954 and 2922 cm^{-1} disappear, indicating that Paraloid B-72 undergoes chain scission. The decrease in absorption bands in the C–H region (2900–2960 cm^{-1}) is a hallmark of the loss of low-molecular-weight components [40,52,67,68]. In contrast, for the orange glass (panel b), the bands at 2954 and 2922 cm^{-1} already disappear after the drop treatment. Moreover, in this case, the bands at 1386 and 1456 cm^{-1} are notably less intense and broader than in the blue glass.

These findings suggest that the tested environmental conditions caused more severe degradation of Paraloid B72 in the orange specimens compared to the blue ones. This difference is likely due to weaker adhesion of the coating on the orange glass. Results are in agreement with SEM observations, where it was evidenced that the acrylic coating exhibited better resistance on the blue glass rather than on the orange one, where it underwent cracking along with further crizzling of the substrate (Figure 7). Paraloid B-72 is known to be affected by UV radiation, similar to other acrylic resins [39,41,69]. UV absorption by the material induces photodegradation, primarily affecting its physicochemical properties and optical characteristics, such as yellowing. In fact, as previously discussed, results from color measurements show that Paraloid B72-coated specimens remained relatively stable after exposure to rainwater and T/RH cycling. However initial signs of yellowing were noticed on the blue specimens upon UVA exposure, as evidenced by an increase in the b* coordinate (Figure S5).

Figures 11 and 12 compare the ATR-FTIR spectra collected for both blue (panels a) and orange (panels b) glass coated with Siox-5 RE20C and Siox-5 RE39, respectively. The bands around 790 and 847 cm^{-1} correspond to Si–O–Si bending vibrations, the shoulder at 940 cm^{-1} is due to the stretching mode of Si–OH, and those at 1038–1024 and 1261 cm^{-1}

are attributed to Si–O–Si stretching modes [70,71]. As previously mentioned, the band near 1640 cm^{-1} is associated with O–H bending [63]. Additionally, the bands at 2854 and 2922 cm^{-1} can be attributed to C–H stretching from organic contamination or residues of the cleaning procedure with ethanol or incomplete polymerization of alkoxide precursors of the sol–gel coating.

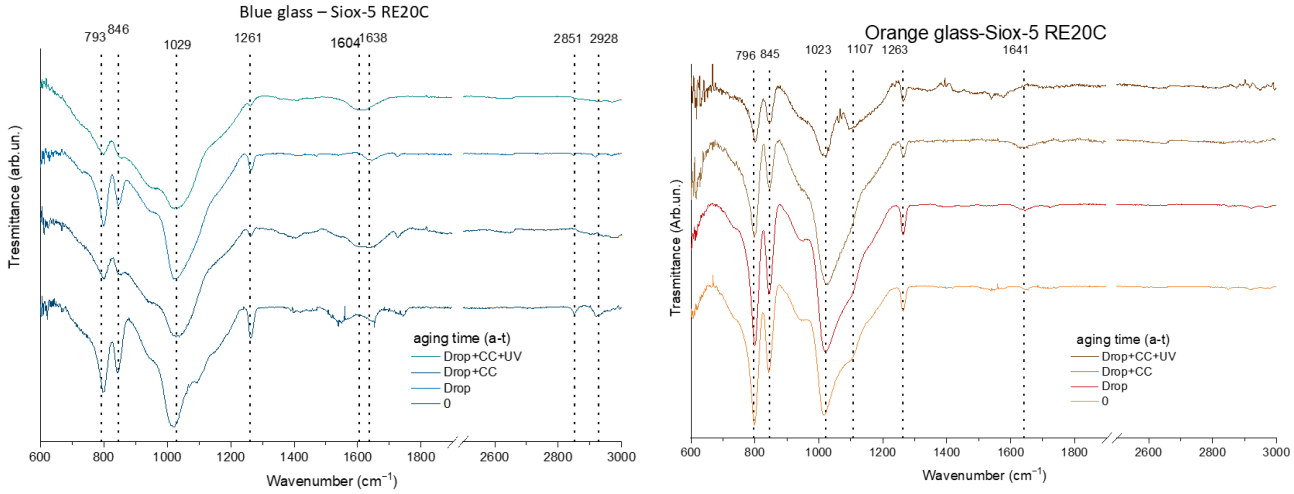

(**a**) (**b**)

Figure 11. ATR FTIR spectra of glass coated with Siox-5 RE20C at different aging times: (**a**) blue glass and (**b**) orange glass.

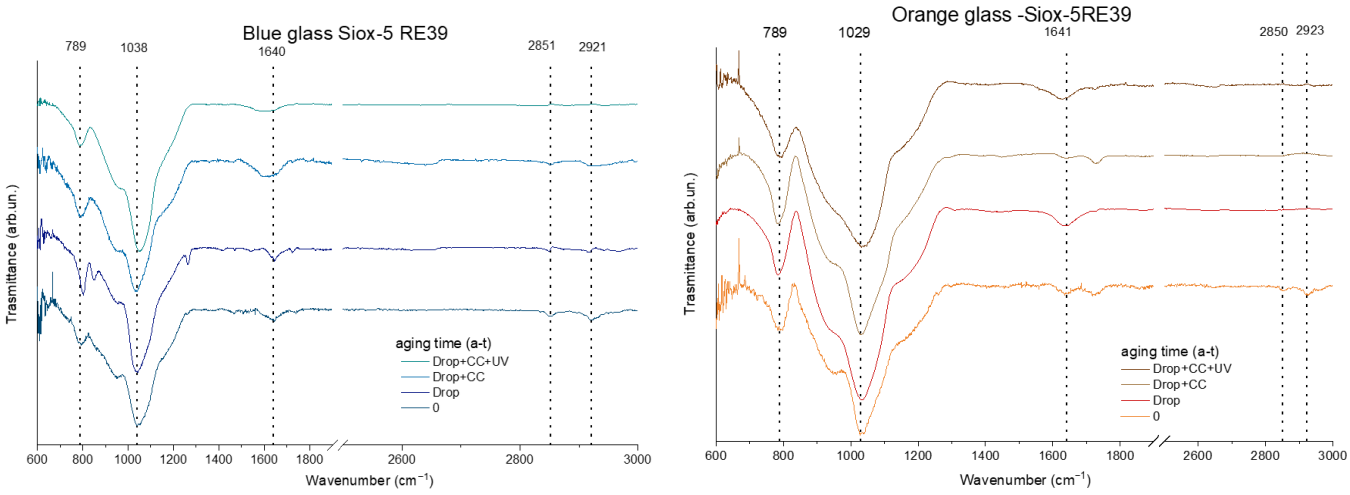

(**a**) (**b**)

Figure 12. ATR FTIR spectra of glass coated with Siox-5 RE39 at different aging times: (**a**) blue glass and (**b**) orange glass.

In Figure 11, panel a, the blue glass spectra show that the bands between 793 and 1261 cm^{-1} became less intense and broader in the Drop+CC+UV specimen compared to the other experimental conditions, suggesting that the UV treatment induces damage to the protective Siox-5 RE20C layer. Moreover, the downshift of the OH band at 1640 cm^{-1} has been observed, as for the uncoated (UT) glass (Figure 9).

On the orange glass (panel b), the artificial aging also caused damage to the protective layer, as the bands at 796 and 786 cm^{-1} become less intense compared to the starting measurement (a-t_0). In addition, the shoulder at 941 cm^{-1} broadens after aging in the

climatic chamber both with and without UV radiation. After CC+UV treatment, the band at 1107 cm^{-1} appears, corresponding to Si–O–Si asymmetric stretching; this behavior is attributed to condensation of silanol groups, which form an open silica network [61].

These findings suggest that Siox-5 RE20C is susceptible to variations in temperature and relative humidity, with a more pronounced effect observed in the blue glass. This behavior is related to a detachment of the consolidant, which was evident in both blue and orange specimens subjected to artificial aging, as can be seen from SEM images (Figures 7 and 8).

In Figure 12, as previously mentioned, the band near 1640 cm^{-1} is associated with O–H bending. However, in the blue specimens treated with Siox-5 RE39, no shift of this band is observed, unlike in the uncoated ones (UT) (Figure 9a) and those treated with Siox-5 RE20C (Figure 11b). In the orange glass, the O–H band is present under all tested conditions in the specimens coated with Siox-5 RE39 (Figure 12b), while it disappears after UV exposure in the uncoated (Figure 9b) and Siox-5 RE20C-coated (Figure 11b) specimens. These results suggest that the Siox-5 RE39 protective treatment provides greater stability compared to the other tested coatings.

It can be seen that, in general, the spectra of both blue and orange glasses coated with Siox-5 RE39 appear very similar across the aging phase. Though some detachment has been observed on blue glass specimens (Figure 8), no chemical modifications appear to have occurred on the coating, suggesting good chemical stability under different conditions of humidity, temperature and UV exposure. The Siox-5 RE39 coating exhibited better adherence compared to the other sol–gel coating tested in this study (Siox-5 RE20C).

3.2.2. Runoff Solutions

According to what was observed and commented on in the pre-aging phase, no statistically significant variations were observed in the pH of the runoff solution, and Si leaching remains undetectable.

For Pb (present only in blue samples), the measured values were always below the limit of detection (LOD 5 ppb). Consequently, it can be concluded that Pb release is negligible, both for untreated samples and for those treated with protective coatings.

Similarly to the pre-aging phase, in the aging phase, the Na concentration was found to not be significantly different from that of the artificial rain solution. However, by examining surface elemental data, it could be hypothesized that some further Na leaching has occurred in blue and orange uncoated (UT) specimens.

Among the elements analyzed, it was possible to quantify K release (Figure 13). Orange specimens were more affected by leaching, showing higher K ion release than the blue ones. No protective coating significantly reduced the release of K from this type of glass.

In contrast, for blue glass, all protective treatments resulted in lower K ion release compared to untreated specimens. Among the tested coatings, Siox-5 RE39 proved to be the most effective, followed by Paraloid B72 and Siox-5 RE20C. The data suggests that, under runoff conditions, the effectiveness of coatings significantly depends on the type of treated glass.

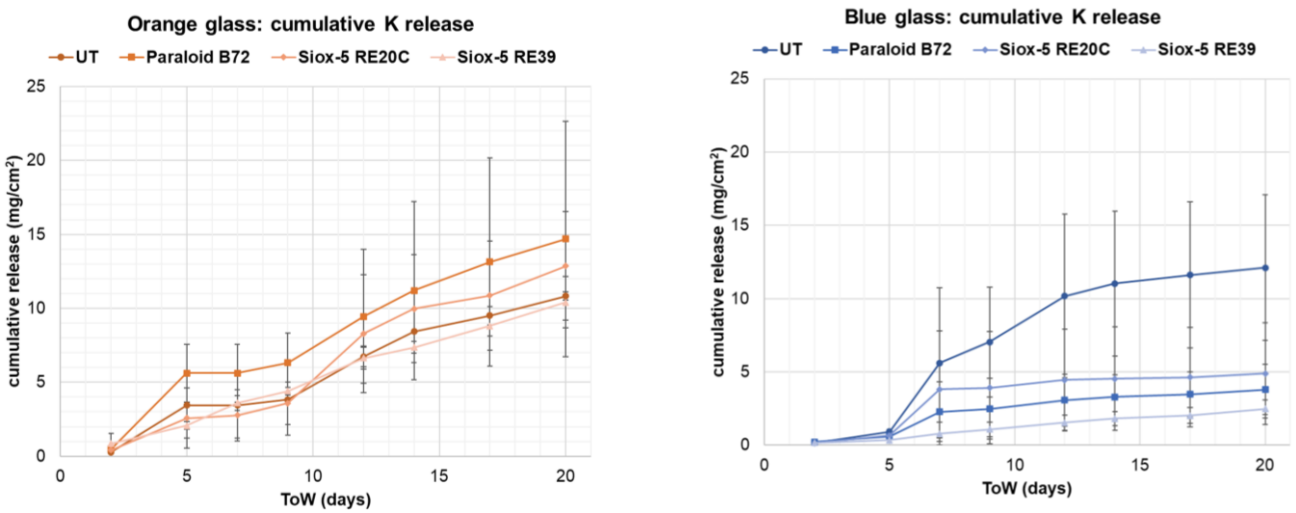

(**a**) (**b**)

Figure 13. K release from coated and uncoated (UT) glass specimens in the aging phase: (**a**) orange glass and (**b**) blue glass. ToW = time of wetness. Error bars represent standard deviation calculated among replicates.

4. Conclusions

This study employed a multi-parameter artificial aging protocol, designed based on real environmental data. The aim was to investigate the weathering of two traditional silicate glasses containing different types and amounts of modifier ions, and to assess the effectiveness of protective coatings when the glasses are exposed to unsheltered and runoff conditions.

The pre-aging phase highlighted that, under acid rain runoff and T/RH cycling conditions, the two glass types developed clearly different weathering patterns. Crizzling emerged on the surface of the orange soda-silicate glass, while the surface of the blue lead glass appeared to remain intact. The better durability of the blue mixed-alkali glass is attributed to the presence of elements like Ca and Pb, which are known to improve glass resistance.

The obtained weathering patterns align well with those found in historical outdoor glass, proving that the aging protocol is effective in replicating natural weathering and providing specimens representative of degraded ancient substrates, suitable for testing coatings' efficiency.

From the subsequent aging phase conducted with a non-acid rain representative of present conditions, it is evident that all the conservative treatments examined (Paraloid B72, Siox-5 RE20C and Siox-5 RE39) are sensible to different degrees to the environmental factors considered in this study: rain runoff, temperature, RH and UVA light.

Paraloid B72 formed a homogeneous coating with good adherence on both glass types; however it was not capable of limiting crizzling on the orange soda-silicate glass, and its performance appears better on more stable smooth glass surfaces. Scission of the acrylic polymer chains occurred on both glass types. Moreover, though the color of the coating remained stable under rain and T and RH cycling exposure, signs of initial yellowing were noticed on the blue glass upon UVA exposure. In light of this, its durability in outdoor environments seems limited.

On the other hand, the sol–gel coatings showed good chemical stability. However, their adhesion to well-preserved, smooth glass surfaces, such as the blue glass ones, appeared to be limited. This was particularly evident for Siox-5 RE20C, and may be ascribed to

the nature of the product, which is marketed as a consolidant and may therefore be more suitable for severely degraded and porous glass substrates.

Indeed, both sol–gel coatings were found to be more effective on the crizzled orange glass. On this substrate, Siox-5 RE39 in particular appears to form a smooth, homogeneous layer with good resistance to accelerated aging under unsheltered runoff conditions.

The findings of this study contribute to the broader discussion on the selection of protective materials for glass heritage conservation, particularly regarding the balance between reversibility and long-term stability. Among tested coatings, Paraloid B72 represents a reversible option. However, this feature, which has long justified its use in conservation, may depend on environmental conditions. When exposed to outdoor environments, the resin tends to undergo structural changes, particularly due to photodegradation, which can compromise its esthetic and protective performance in the long term. In contrast, Siox-5 RE20C and Siox-5 RE39 consolidants, based on sol–gel technology, cannot be considered completely reversible as their mechanism of action involves the formation of a silica-based network; the removal of this layer could induce damage to the underlying historical glass. Nevertheless, this provides chemical and structural compatibility with the glass substrate. The choice between products aimed at the conservation of glass should thus be guided by the specific conservation context, prioritizing reversibility in controlled environments, and stability in more aggressive exposed conditions.

Supplementary Materials: The following supporting information can be downloaded at: https://www.mdpi.com/article/10.3390/heritage9010002/s1, Figure S1: Variation in L*, a*, b* parameters during pre-aging; Figure S2: secondary electron image showing nitrate salt deposits on orange glass during pre-aging; Figure S3: Variation in L*, a*, b* parameters caused by the application of protective coatings; Figure S4: Variation in L*, a*, b* parameters during aging of orange glass coated and uncoated; Figure S5: Variation in L*, a*, b* parameters during aging of blue glass coated and uncoated.

Author Contributions: Conceptualization, E.B., M.V. and C.C.; Methodology, E.B. and C.C.; Validation, E.B., T.S. and C.C.; Formal Analysis, S.S., E.T. and M.Z.; Investigation, S.S., E.B. and M.Z.; Data Curation, S.S. and E.T.; Writing—Original Draft Preparation, S.S., E.T. and M.Z.; Writing—Review and Editing, E.B., T.S., M.V. and C.C.; Visualization, E.T. and M.Z.; Supervision, E.B. and C.C.; Project Administration, M.V. and C.C.; Funding Acquisition, M.V. and C.C. All authors have read and agreed to the published version of the manuscript.

Funding: The project is funded by the European Union—NextGenerationEU under the National Recovery and Resilience Plan (PNRR)—Mission 4 Education and research—Component 2 From research to business—Investment 1.3, Notice D.D. 341 of 15 March 2022, entitled: Cultural Heritage Active Innovation for Sustainable Society proposal code PE0000020—CUPJ33C22002850006, duration until 28 February 2026. The project was also supported by the Alma Idea Grant 2022, a program funded by the University of Bologna to support basic research.

Data Availability Statement: The original contributions presented in this study are included in the article/Supplementary Material. The dataset related to color, SEM/EDS and FTIR-ATR analyses is available at https://doi.org/10.6092/unibo/amsacta/8588. Further inquiries can be directed to the corresponding authors.

Acknowledgments: The authors would like to thank Francesca Ospitali for lending her expertise in SEM/EDS analysis.

Conflicts of Interest: The authors declare no conflicts of interest. The funders had no role in the design of the study; in the collection, analyses, or interpretation of data; in the writing of the manuscript; or in the decision to publish the results.

Abbreviations

The following abbreviations are used in this manuscript:

UT	Untreated, uncoated glass
drop	Dripping test simulating rain runoff
CC	Climatic chamber
BO	Bridging oxygen
NBO	Non bridging oxygen

References

1. Scholze, H. *Glass: Nature, Structure, and Properties*; Springer: New York, NY, USA, 1991; ISBN 978-1-4613-9069-5.
2. Davison, S.; Newton, R.G. *Conservation and Restoration of Glass*, 2nd ed.; Routledge, Taylor and Francis: London, UK, 2008; ISBN 978-0-08-056931-4.
3. Zanini, R.; Fransceschin, G.; Cattaruzza, E.; Travigilia, A. A Review of Glass Corrosion: The Unique Contribution of Studying Ancient Glass to Validate Glass Alteration Models. *npj Mater. Degrad.* **2023**, *7*, 38. [CrossRef]
4. Fernández–Navarro, J.; Villegas, M. What Is Glass?: An Introduction to the Physics and Chemistry of Silicate Glasses. In *Modern Methods for Analysing Archaeological and Historical Glass*; Janssens, K., Ed.; Wiley: Hoboken, NJ, USA, 2013; pp. 1–22, ISBN 978-0-470-51614-0.
5. Verità, M. Il Vetro: Proprietà, Resistenza Chimica e Processi Di Alterazione. In *Mosaici Medievali a Roma Attraverso il Restauro Dell'ICR 1991–2004*; Gangemi: Rome, Italy, 2017; pp. 507–516.
6. Tite, M.S.; Freestone, I.; Mason, R.; Molera, J.; Vendrell-Saz, M.; Wood, N. Lead Glazes in Antiquity—Methods of Pro-duction and Reasons for Use. *Archaeometry* **1998**, *40*, 241–260. [CrossRef]
7. Caurant, D.; Wallez, G.; Majérus, O.; Roisine, G.; Charpentier, T. Structure and Properties of Lead Silicate Glasses. In *Lead in Glassy Materials in Cultural Heritage*; Wiley: Hoboken, NJ, USA, 2024; pp. 35–92, ISBN 978-1-394-26541-1.
8. Melcher, M.; Schreiner, M. Glass Degradation by Liquids and Atmospheric Agents. In *Modern Methods for Analysing Archaeological and Historical Glass*; Janssens, K., Ed.; Wiley: Hoboken, NJ, USA, 2013; pp. 609–651, ISBN 978-0-470-51614-0.
9. Melcher, M.; Schreiner, M. Leaching Studies on Naturally Weathered Potash-Lime–Silica Glasses. *J. Non-Cryst. Solids* **2006**, *352*, 368–379. [CrossRef]
10. Alloteau, F.; Lehuédé, P.; Majérus, O.; Biron, I.; Dervanian, A.; Charpentier, T.; Caurant, D. New Insight into Atmospheric Alteration of Alkali-Lime Silicate Glasses. *Corros. Sci.* **2017**, *122*, 12–25. [CrossRef]
11. Alloteau, F.; Majérus, O.; Biron, I.; Lehuédé, P.; Caurant, D.; Charpentier, T.; Seyeux, A. Temperature-Dependent Mechanisms of the Atmospheric Alteration of a Mixed-Alkali Lime Silicate Glass. *Corros. Sci.* **2019**, *159*, 108129. [CrossRef]
12. Carmona, N.; García-Heras, M.; Gil, C.; Villegas, M.A. Chemical Degradation of Glasses under Simulated Marine Medium. *Mater. Chem. Phys.* **2005**, *94*, 92–102. [CrossRef]
13. Asay, D.B.; Seong, K.M. Evolution of the Adsorbed Water Layer Structure on Silicon Oxide at Room Temperature. *J. Phys. Chem. B* **2005**, *109*, 16760–16763. [CrossRef]
14. Schalm, O.; Nuyts, G.; Janssens, K. Some Critical Observations about the Degradation of Glass: The Formation of Lamellae Explained. *J. Non-Cryst. Solids* **2021**, *569*, 120984. [CrossRef]
15. Sinton, C.W.; LaCourse, W.C. Experimental Survey of the Chemical Durability of Commercial Soda-Lime-Silicate Glasses. *Mater. Res. Bull.* **2001**, *36*, 2471–2479. [CrossRef]
16. El-Shamy, T.M.; Morsi, S.E.; Taki-Eldin, H.D.; Ahemd, A.A. Chemical Durability of Na_2O CaO SiO_2 Glasses in Acid Solutions. *J. Non-Cryst. Solids* **1975**, *19*, 241–250. [CrossRef]
17. Bunker, B.C. Molecular Mechanisms for Corrosion of Silica and Silicate Glasses. *J. Non-Cryst. Solids* **1994**, *179*, 300–308. [CrossRef]
18. Jantzen, C.M.; Plodinec, M.J. Thermodynamic Model of Natural, Medieval and Nuclear Waste Glass Durability. *J. Non-Cryst. Solids* **1984**, *67*, 207–223. [CrossRef]
19. Centenaro, S.; Fransceschin, G.; Cattaruzza, E.; Travigilia, A. Consolidation and Coating Treatments for Glass in the Cultural Heritage Field: A Review. *J. Cult. Heirtage* **2023**, *64*, 132–143. [CrossRef]
20. Moncrieff, A. Problems and Potentialities in the Conservation of Vitreous Materials. *Stud. Conserv.* **1975**, *20*, 99–104. [CrossRef]
21. Ntasi, G.; Sbriglia, S.; Pitocchi, R.; Vinciguerra, R.; Melchiorre, C.; Dello Ioio, L.; Fatigati, G.; Crisci, E.; Bonaduce, I.; Carpentieri, A.; et al. Proteomic Characterization of Collagen-Based Animal Glues for Restoration. *J. Proteome Res.* **2022**, *21*, 2173–2184. [CrossRef]
22. Davison, S. A Review of Adhesives and Consolidants Used on Glass Antiquities. *Stud. Conserv.* **1984**, *29*, 191–194. [CrossRef]
23. Zhao, X.; Li, X.; Zhang, S.; Niu, Q.; Li, Z.; Xue, C. Investigation of Whitening Mechanism on Cultural Relic Surfaces Treated with Paraloid B72. *Coatings* **2024**, *14*, 1240. [CrossRef]

24. Artesani, A.; Di Turo, F.; Zucchelli, M.; Traviglia, A. Recent Advances in Protective Coatings for Cultural Heritage—An Overview. *Coatings* **2020**, *10*, 217. [CrossRef]
25. Carmona, N.; Wittstadt, K.; Römich, H. Consolidation of Paint on Stained Glass Windows: Comparative Study and New Approaches. *J. Cult. Heirtage* **2009**, *10*, 403–409. [CrossRef]
26. De Bardi, M.; Hutter, H.; Schreiner, M.; Bertoncello, R. Potash-Lime-Silica Glass: Protection from Weathering. *Herit. Sci.* **2015**, *3*, 22. [CrossRef]
27. Dal Bianco, B.; Bertoncello, R.; Bouquillon, A.; Dran, J.-C.; Milanese, L.; Roehrs, S.; Sada, C.; Salomon, J.; Voltolina, S. Investigation on Sol–Gel Silica Coatings for the Protection of Ancient Glass: Interaction with Glass Surface and Protection Efficiency. *J. Non-Cryst. Solids* **2008**, *354*, 2983–2992. [CrossRef]
28. Cecchin, M.; Bortolussi, C. La tecnologia sol-gel per la protezione della ceramica. In *Il Restauro della Ceramica: Studio dei Materiali e delle Forme di Degrado, Progettazione di Iinterventi di Restauro e Conservazione: Giornata di Studio, MIC Museo Internazionale delle Ceramiche in Faenza, 29 Novembre 2019*; Faenza Bollettino del Museo Internazionale delle Ceramiche in Faenza; Edizioni Polistampa: Firenze, Italy, 2019; pp. 74–82, ISBN 978-88-596-2059-4.
29. Stoveland, L.P.; Ormsby, B.; Stols-Witlox, M.; Streeton, N.L.W. Mock-Ups and Materiality in Conservation Research. In *Transcending Boundaries: Integrated Approaches to Conservation; ICOM-CC 19th Triennial Conference Preprints, Beijing, China, 17–21 May 2021*; International Council of Museums: Paris, France, 2023; ISBN 978-2-491997-14-4.
30. Dillis, S.; Van Ham-Meert, A.; Leeming, P.; Shortland, A.J.; Gobejishvili, G.; Abramishvili, M.; Degryse, P. Antimony as a Raw Material in Ancient Metal and Glass Making: Provenancing Georgian LBA Metallic Sb by Isotope Analysis. *STAR Sci. Technol. Archaeol. Res.* **2019**, *5*, 98–112. [CrossRef]
31. Freestone, I.; Stapleton, C.P. Composition Technology and Production of Coulerd Glasse from Roman Mosaic Vesseld. In *Glass of the Roman World*; Oxbow Books: Oxford, UK, 2015; pp. 62–67.
32. Shortland, A.J. The Use and the Origin of Antimonate Colorants in Early Egyptian Glass. *Archeometry* **2002**, *44*, 527–530. [CrossRef]
33. Costa, M.; Arruda, A.M.; Dias, L.; Barbosa, R.; Mirão, J.; Vandenabeele, P. The Combined Use of Raman and micro-X-ray Diffraction Analysis in the Study of Archaeological Glass Beads. *J. Raman Spectrosc.* **2019**, *50*, 250–261. [CrossRef]
34. Yatsuk, O.; Fiocco, G.; Malagodi, M.; Re, A.; Lo Giudice, A.; Iaia, C.; Gulmini, M. The Non-Invasive Characterization of Iron Age Glass Finds from the "Gaetano Chierici" Collection in Reggio Emilia (Italy). *Heritage* **2023**, *6*, 5583–5606. [CrossRef]
35. Constantinescu, B.; Cristea-Stan, D.; Szokefalvi-Nagy, Z.; Kovács, I.; Harsányi, I. PIXE and PGAA–Complementary Methods for Studies on Ancient Glass Artefacts (from Byzantine, Late Medieval to Modern Murano Glass). *Nucl. Instrum. Methods Phys. Res. B Beam Interact. Mater. At.* **2018**, *417*, 105–109. [CrossRef]
36. Bortolussi, C.; Cecchin, M.; Checcucci, B.; Poggi, S. Conservazione preventiva ed innovazione: La tecnica sol-gel per le opere di Sosabravo e Carlè ad Albisola Superiore. In *La Conservazione della Ceramica All'aperto: II Giornata di Studio, 10 giugno 2021*; Faenza Bollettino del Museo Internazionale delle Ceramiche in Faenza; Edizioni Polistampa: Firenze, Italy, 2021; pp. 115–123, ISBN 978-88-596-2189-8.
37. Vella, S.; Bortolussi, C.; Zanardi, B. The Eternal Youth of Capalbio's *Monsters*: A Planned Preventive Conservation Project. In *The Conservation of Sculpture Parks*; Archetype Publications Ltd.: London, UK, 2018; pp. 84–97.
38. Technical Data Sheet: Siox-5 RE20C 2025, SILTEA SRL Via Carlo Goldoni 18, Padova 35131 PD, Italia. Available online: https://www.siltea.eu/wp-content/uploads/2025/02/CONSOLIDANTE-SIOX-5-RE20C-SCHEDA-TECNICA.pdf (accessed on 7 August 2025).
39. Kotlík, P.; Doubravová, K.; Jiˇrí, H.; Lubomír, K.; Jiˇrí, A. Acrylic Copolymer Coatings for Protection against UV Rays. *J. Cult. Herit* **2014**, *15*, 44–48. [CrossRef]
40. Scalarone, D.; Lazzari, M.; Chiantore, O. Acrylic Protective Coatings Modified with Titanium Dioxide Nanoparticles: Comparative Study of Stability under Irradiation. *Polym. Degrad. Stab.* **2012**, *97*, 2136–2142. [CrossRef]
41. Chapman, S.; Mason, D. Literature Review: The Use of Paraloid B-72 as a Surface Consolidant for Stained Glass. *J. Am. Inst. Conserv.* **2003**, *42*, 381–392. [CrossRef]
42. Koob, S.P. The Use of Paraloid B-72 as an Adhesive: Its Application for Archaeological Ceramics and Other Materials. *Stud. Conserv.* **1986**, *31*, 7–14. [CrossRef]
43. Koob, S.P. *Conservation and Care of Glass Objects*; Archetype Publications: London, UK; The Corning Museum of Glass: Corning, NY, USA, 2006.
44. Bernardi, E.; Chiavari, C.; Lenza, B.; Martini, C.; Morselli, L.; Ospitali, F.; Robbiola, L. The Atmospheric Corrosion of Quaternary Bronzes: The Leaching Action of Acid Rain. *Corros. Sci.* **2009**, *51*, 159–170. [CrossRef]
45. Spadavecchia, S.; Chiavari, C.; Ospitali, F.; Gualtieri, S.; Hillar, A.C.; Bernardi, E. Evaluation of the Effectiveness of Coatings for the Protection of Outdoor Terracotta Artworks through Artificial Ageing Tests. *J. Cult. Herit* **2024**, *70*, 213–222. [CrossRef]
46. Chiavari, C.; Bernardi, E.; Martini, C.; Passarini, F.; Ospitali, F.; Robbiola, L. The Atmospheric Corrosion of Quaternary Bronzes: The Action of Stagnant Rain Water. *Corros. Sci.* **2010**, *52*, 3002–3010. [CrossRef]

47. Morselli, L.; Bernardi, E.; Vassura, I.; Passarini, F.; Tesini, E. Chemical Composition of Wet and Dry Atmospheric Depositions in an Urban Environment: Local, Regional and Long-Range Influences. *J. Atmos. Chem.* **2008**, *59*, 151–170. [CrossRef]
48. Timoncini, A.; Brattich, E.; Bernardi, E.; Chiavari, C.; Tositti, L. Safeguarding Outdoor Cultural Heritage Materials in an Ever-Changing Troposphere: Challenges and New Guidelines for Artificial Ageing Test. *J. Cult. Herit* **2023**, *59*, 190–201. [CrossRef]
49. Camuffo, D.; Della Valle, A.; Becherini, F. A Critical Analysis of One Standard and Five Methods to Monitor Surface Wetness and Time-of-Wetness. *Theor. Appl. Clim.* **2018**, *132*, 1143–1151. [CrossRef]
50. Rodrigues, J.D.; Grossi, A. Indicators and Ratings for the Compatibility Assessment of Conservation Actions. *J. Cult. Herit.* **2007**, *8*, 32–43. [CrossRef]
51. Rogers, G. Transparent Coating on a Color Surface. *J. Opt. Soc. Am. A* **2024**, *41*, 1215. [CrossRef]
52. Oancea, A.V.; Bodi, G.; Cernescu, A.; Spiridon, I.; Nicolescu, A.; Drobota, M.; Cotofana, C.; Simionescu, B.C.; Olaru, M. Protective Coatings for Ceramic Artefacts Exposed to UV Ageing. *npj Mater. Degrad.* **2023**, *7*, 21. [CrossRef]
53. Gueli, A.M.; Pasquale, S.; Tanasi, D.; Hassam, S.; Lemasson, Q.; Moignard, B.; Pacheco, C.; Stella, G.; Politi, G. Weathering and Deterioration of Archeological Glasses from Late Roman Sicily. *Int. J. Appl. Glass Sci.* **2020**, *11*, 215–225. [CrossRef]
54. Kunicki-Goldfinger, J.J. Unstable Historic Glass: Symptoms, Causes, Mechanisms and Conservation. *Stud. Conserv.* **2008**, *53*, 47–60. [CrossRef]
55. Brill, R.H. CRIZZLING–A PROBLEM IN GLASS CONSERVATION. *Stud. Conserv.* **1975**, *20*, 121–134. [CrossRef]
56. Andrews, A.I.; Clark, G.L.; Alexander, H.W. THE DETERMINATION BY X-RAY METHODS OF CRYSTALLINE COMPOUNDS CAUSING OPACITY IN ENAMELS. *J. Am. Ceram. Soc.* **1933**, *16*, 385–392. [CrossRef]
57. Robinet, L.; Hall, C.; Eremin, K.; Fearn, S.; Tate, J. Alteration of Soda Silicate Glasses by Organic Pollutants in Museums: Mechanisms and Kinetics. *J. Non-Cryst. Solids* **2009**, *355*, 1479–1488. [CrossRef]
58. Angeli, F.; Brunswic, L.; Charpentier, T.; Gin, S. Lead Leaching in Industrial Crystal Glasses. In *Lead in Glassy Materials in Cultural Heritage*; John Wiley & Sons, Ltd.: Hoboken, NJ, USA, 2024; pp. 295–330, ISBN 978-1-394-26541-1.
59. Jialiang, Y. Further Studies on the IR Spectra of Silicate Glasses. *J. Non-Cryst. Solids* **1986**, *84*, 114–119. [CrossRef]
60. Handke, M.; Mozgawa, W.; Nocuń, M. Specific Features of the IR Spectra of Silicate Glasses. *J. Mol. Struct.* **1994**, *325*, 129–136. [CrossRef]
61. Laso, E.; Aparicio, M.; Palomar, T. Influence of Humidity in the Alteration of Unstable Glasses. *Int. J. Appl. Glass Sci.* **2024**, *15*, 88–103. [CrossRef]
62. Gussoni, M.; Castiglioni, C. Infrared Intensities. Use of the CH-Stretching Band Intensity as a Tool for Evaluating the Acidity of Hydrogen Atoms in Hydrocarbons. *J. Mol. Struct.* **2000**, *521*, 1–18. [CrossRef]
63. Peyvandi, A.; Holmes, D.; Soroushian, P.; Balachandra, A.M. Monitoring of Sulfate Attack in Concrete by Al27 and Si29 MAS NMR Spectroscopy. *J. Mater. Civ. Eng.* **2015**, *27*, 04014226. [CrossRef]
64. Sheth, N.; Ngo, D.; Banerjee, J.; Zhou, Y.; Pantano, C.G.; Kim, S.H. Probing Hydrogen-Bonding Interactions of Water Molecules Adsorbed on Silica, Sodium Calcium Silicate, and Calcium Aluminosilicate Glasses. *J. Phys. Chem. C* **2018**, *122*, 17792–17801. [CrossRef]
65. Lynch, M.E.; Folz, D.C.; Clark, D.E. Use of FTIR Reflectance Spectroscopy to Monitor Corrosion Mechanisms on Glass Surfaces. *J. Non-Cryst. Solids* **2007**, *353*, 2667–2674. [CrossRef]
66. Pintus, V.; Wei, S.; Schreiner, M. UV Ageing Studies: Evaluation of Lightfastness Declarations of Commercial Acrylic Paints. *Anal. Bioanal. Chem.* **2012**, *402*, 1567–1584. [CrossRef]
67. Lamuraglia, R.; Campostrini, A.; Ghedini, E.; De Lorenzi Pezzolo, A.; Di Michele, A.; Franceschin, G.; Menegazzo, F.; Signoretto, M.; Traviglia, A. A New Green Coating for the Protection of Frescoes: From the Synthesis to the Performances Evaluation. *Coatings* **2023**, *13*, 277. [CrossRef]
68. Chiantore, O.; Lazzari, M. Photo-Oxidative Stability of Paraloid Acrylic Protective Polymers. *Polymer* **2001**, *42*, 17–27. [CrossRef]
69. Brandt, J.; Kanaki, E.; Fischer, D.; Herm, C. Evaluation of the Composition, Thermal and Mechanical Behavior, and Color Changes of Artificially and Naturally Aged Polymers for the Conservation of Stained Glass Windows. *Polymers* **2023**, *15*, 2595. [CrossRef] [PubMed]
70. Mandracci, P.; Mussano, F.; Ceruti, P.; Pirri, C.F.; Carossa, S. Reduction of Bacterial Adhesion on Dental Composite Resins by Silicon–Oxygen Thin Film Coatings. *Biomed. Mater.* **2015**, *10*, 015017. [CrossRef]
71. Katayama, Y.; Ando, E.; Kawaguchi, T. Characterization of SiO_2 Films on Glass Substrate by Sol-Gel and Vacuum Deposition Methods. *J. Non-Cryst. Solids* **1992**, *147–148*, 437–441. [CrossRef]